Live imaging of the *Cryptosporidium parvum* lifecycle reveals direct development of male and female gametes from type one meronts

Elizabeth D. English[1], Amandine Guérin[1], Jayesh Tandel[1], and Boris Striepen[1]*

[1] Department of Pathobiology, School of Veterinary Medicine, University of Pennsylvania, Philadelphia, Pennsylvania, United States of America

* Corresponding author

Email: striepen@upenn.edu (BS)

Short title: The *Cryptosporidium* lifecycle

Abstract

Cryptosporidium **is a leading infectious cause of diarrhea around the world associated with waterborne outbreaks, community spread, or zoonotic transmission. The parasite has significant impact on early childhood mortality, and infection is both consequence and cause of malnutrition and stunting. There is currently no vaccine, and treatment options are very limited.** ***Cryptosporidium*** **is a member of the Apicomplexa, and as typical for this protist phylum relies on asexual and sexual reproduction. In contrast to other Apicomplexa, like malaria parasite** ***Plasmodium, Cryptosporidium's*** **entire lifecycle unfolds in a single host in less than three days. Here we establish a model to image lifecycle progression in living cells, and observe, track, and compare nuclear division of asexual and sexual stage parasites. We establish the length and sequence of the cell cycles of all stages and map the developmental fate of parasites across multiple rounds of invasion and egress. We determine that the parasite executes an intrinsic program of three generations of asexual replication, followed by a single generation of sexual stages that is independent of environmental stimuli. We find no evidence for a morphologically distinct intermediate stage (the tetraploid type II meront) but demonstrate direct development of gametes from 8N type I meronts. The progeny of each meront is collectively committed to either asexual or sexual fate, but importantly, meronts committed to sexual fate give rise to both males and females. We define a** ***Cryptosporidium*** **lifecycle matching Tyzzer's original description and inconsistent with the coccidian lifecycle now shown in many textbooks.**

Introduction

Pathogen associated diarrheal disease is one of the leading causes of mortality in children under the age of 5 years [1]. While efforts to improve sanitation, hygiene and access to clean

water have reduced the number of diarrheal deaths, nearly half a million children under the age of 5 died due to diarrheal diseases in 2015. The three most common causes of pathogen associated diarrhea in children under 5 are rotavirus, *Cryptosporidium*, and *Shigella*, which together account for more than half of all diarrheal deaths in this age group [1, 2]. Malnourished children are particularly susceptible to severe cryptosporidiosis [2-4], and in turn, infection with this pathogen can have long lasting consequences for the nutritional status and overall growth and development of children [5, 6]. Children develop non-sterile immunity to *Cryptosporidium* that protects from severe disease and malnutrition [7], however this immunity is slow to develop and currently no vaccines are available to prevent the infection [3]. Nitazoxanide has been approved by the US Food and Drug Administration for the treatment of cryptosporidiosis, but this drug is not effective in immunocompromised or malnourished individuals [8]. The last five years have seen a significant push towards better treatments for cryptosporidiosis (see [9] for a succinct review). Several of these efforts took advantage of recent advances in the development of antimalarials by using cherry picked compound collections initially derived in phenotypic screens against *Plasmodium falciparum* [10-15]. The value of targeting multiple lifecycle stages is a clear lesson that emerged from the malaria drug development effort [16]. A more comprehensive understanding of the biology of the *Cryptosporidium* lifecycle and the relative susceptibility of its different segments is required to discover and improve drugs to establish effective treatments for this disease [3].

Cryptosporidium is a single cell protist parasite and a member of the phylum Apicomplexa, organisms that undergo complex lifecycles of asexual and sexual reproduction. In the well-studied apicomplexans *Plasmodium* and *Toxoplasma* (the causative agents of malaria and toxoplasmosis), this lifecycle unfolds in different hosts: mice and cats or humans and mosquitoes, respectively. In contrast, *Cryptosporidium* replicates both asexually and sexually within a single

host and transmission between hosts occurs through meiotic spores called oocysts. In humans and animals, *Cryptosporidium* infects the intestinal epithelium and oocyst shedding begins on the third day of infection, in the absence of cell mediated immunity infection is chronic and parasite growth continues unabated [17-19]. Here we study *Cryptosporidium parvum*, a parasite of cattle and humans that is experimentally tractable [20]. At any given time, roughly one third of the parasites within the small intestine of an infected mouse replicate asexually, one third appear to be sexual stages, and one third represent post-fertilization stages that are in the process of forming oocysts [21]. In cell culture systems, including the widely used human adeno carcinoma cell line HCT-8, *Cryptosporidium* is limited to approximately 3 days of growth. Inoculation of HCT-8 cells with oocysts or sporozoites released from oocysts produces robust infection with parasites that reproduce asexually, however after two days the culture abruptly sexualizes and is dominated by male and female gametes and growth ceases. Post-fertilization stages are not observed in culture, likely due to a block in the fertilization step [21]. Interestingly, in organoid-based cultures longer-term growth has been observed as has fertilization and oocyst formation [22-24]. Sex thus appears to reset the lifecycle and initiate subsequent rounds of asexual growth and expansion.

Different apicomplexans have evolved diverging mechanisms to accommodate the progression of developmental stages to their respective host niches. Commitment to sexual development in *Plasmodium* occurs at varying frequencies depending on species and strain, suggesting an underlying inherited developmental threshold [25]. A small portion of each asexual generation commits to sexual development and initiates gametocyte development, these cells will mature into gametes once ingested by mosquitoes with a bloodmeal and then undergo fertilization [26]. Tissue and biochemical cues have been identified that impact on the likelihood of the developmental switch that results in exit from the asexual cell cycle and differentiation into the growth arrested gametocyte stage [27, 28]. In contrast, conversion of *Hammondia* from fast

93 growing tachyzoites to slow growing bradyzoites appears to be governed by a molecular clock
94 [29, 30]. Similarly, *Eimeria* executes a predetermined number of asexual cycles prior to the
95 emergence of gametes [31, 32].
96
97 The *Cryptosporidium* lifecycle is remarkably short and much of it unfolds in tissue culture.
98 Here we establish a long-term live-cell microscopy model to directly observe the lifecycle and to
99 fate map developmental progression. We find no evidence of environmental induction of
100 gametogenesis, but strict adherence to a timed developmental program. The intracellular
101 development of all stages unfolds in roughly twelve-hour intervals, with three generations of
102 asexual meronts followed by a single generation of gametes. Merozoites emerging from one
103 parasite cell are collectively committed to either an asexual or sexual fate, but sexually committed
104 meronts give rise to both males and females. We rigorously demonstrate that gametes develop
105 directly from asexual stages that produce eight merozoites, known as type I meronts, and we
106 refute a role for a morphologically distinct type II meront as an intermediate stage between the
107 asexual and the sexual phase of *Cryptosporidium* development.
108
109 **Results**
110 **Sexual differentiation of *Cryptosporidium parvum* follows a parasite intrinsic program**
111 *Cryptosporidium parvum* differentiates from the asexual to sexual phase of its lifecycle 48
112 hours into culture and parasites cease to replicate. We wondered how this transition may be
113 triggered and considered the presence of a parasite extrinsic stimulus (Fig 1A). This might include
114 changes in the physicochemical properties of the environment [33], the depletion or accumulation
115 of a metabolite [27, 34], or the activity of a dedicated density-dependent quorum sensing
116 mechanism [35]. Alternatively, *C. parvum* may follow an intrinsic program that is independent of
117 extracellular factors. To test for differentiation stimuli, we performed experiments with conditioned

media (Fig 1B). Media were conditioned by growing HCT-8 cells with or without *C. parvum* infection for 48 hours, the time point when differentiation occurs. The media was filtered (0.45 μm) to remove extracellular parasites, and then transferred to fresh cultures. These cultures were infected with a *C. parvum* reporter line expressing nanoluciferase and we monitored parasite growth over 72 hours by luciferase assay [20]. Use of infection conditioned media did not result in an earlier arrest of parasite growth (Fig 1C).

We also conducted experiments using a *C. parvum* reporter strain [21] and recorded the developmental progression through different stages. We again used conditioned media, this time added to infected coverslip cultures, which were processed for immunofluorescence assays 24, 48, and 72 hours after infection. The number of male gamonts (blue), female gametes (pink) and asexual meronts (green) was scored at each time point by microscopy (n=3) and is displayed as a fraction of all parasites encountered (Fig 1D). Conditioning did not hasten lifecycle progression and the representation of different stages was indistinguishable between conditioned and unconditioned media, and similar to that previously reported [21].

We considered that a sex inducing factor might be unstable, poorly soluble, or remain cell associated, and thus is not transmitted well by media transfer. We used superinfection of the same culture to test this (Fig 1E). Host cells were first infected with unmarked wildtype *C. parvum*, 24 hours later they were infected again, this second time with a transgenic parasite strain expressing a fluorescent reporter. We then performed immunofluorescence assays to score stages and assessed life cycle progression of both infections separately. Despite the presence of a sexualized primary infection, the second infection again produced gametes only after 48 hours (Fig 1F), both waves showed similar kinetics but were offset by their 24 hours difference of time

in culture. Taken together, we did not find evidence for an external induction mechanism, and thus propose that *C. parvum* is following an intrinsic program of lifecycle progression.

Imaging the intracellular development of asexual and sexual stages of *C. parvum*

Next, we wanted to observe the *C. parvum* lifecycle program in real time by live-cell microscopy. We engineered parasites to express a mScarlet fluorescent protein in the cytoplasm in addition to a mNeon-tagged H2B histone labeling the nuclei in green (S1 Fig). These parasites were used to infect HCT-8 cells grown in 8-well chamber slides and imaged using an GE DeltaVision OMX Structured Illumination Microscope controlling temperature and atmosphere (see Materials and Methods for detail). In preliminary experimentation, we established that imaging every 30 minutes permitted continuous recording for up to 42 hours while maintaining parasite and host cell viability. We began imaging at 11 hours of culture which we had previously established as the end of the first sporozoite initiated merogony cycle [36] and also conducted experiments imaging from 29 or 40 hours of culture onwards. We used multiple point visiting and autofocus routines to allow us to observe cells in parallel and in significant numbers collecting a total of 6171 hours of time lapse data, of which 4542.5 hours were suitable for analysis. We were able to consistently distinguish the intracellular development of asexual meronts, from that of male gamonts and female gametes. Asexual parasites were observed prior to 40 hours post infection, sexual stages after that point.

Figure 2A shows selected still images from two representative movies of asexual development (see S1 Movie for multiple additional cells). We analyzed the intracellular development of a total of 380 meronts and found a mean time to egress of 12.57 hours, which is similar to the timing of sporozoite initiated *C. parvum* merogony [36]. *C. parvum* replicates by schizogony [37], resulting in a cell with eight nuclei. We found that the increase in the number of

nuclei strictly followed geometric progression, indicating that in contrast to *Plasmodium* [38], in *C. parvum* nuclear divisions are highly coordinated and synchronous throughout. Using nuclear divisions as landmarks, we decerned three phases: a long initial establishment phase, a relatively brief mitotic phase, and a final budding phase. Meronts completed the first nuclear division after 7.92 hours, and then ran through two additional complete mitotic cycles, taking about 1 hour for each (Fig 2C, D and E). There was a lag phase of 2.77 hours between the last division and egress.

The development of male gamonts followed a pattern similar to that of meronts (Fig 2B and S2 Movie). After a 6.28-hour establishment phase, four rapid mitotic cycles produced 16 nuclei, and the average time to egress was 12.08 hours (Fig 2F, G and H). Up to the 8N stage, the nuclei of male gamonts were round; only the last division produced the highly condensed spindle shaped nuclei, that are characteristic for male gametes [39, 40]. As seen for meronts the time required increased slightly from division to division (Fig. 2F). While immature male gamonts appeared overall similar to meronts, they can be distinguished. The nuclei of gamonts clustered to the center, while nuclei of meronts showed greater dispersion (see S2 Fig). We note that half of the male parasites observed failed to egress (93 out of 172 times), this may be typical for male gamonts, associated with the culture model, or could reflect additive photodamage due to longer overall imaging times.

Female parasites did not undergo nuclear division and remained intracellular, allowing us to image them for 24 hours (the time the experiment ended). However, the size of their nuclei increased 3-4 times in area, and the overall size of the gamete grew 6-8 times in this time (Fig 2I, J and S3 Movie). We made two additional observations. First, while female gametes grew rapidly initially, growth plateaued after 12-15 hours. Female gametes are the transcriptionally and translationally most active of all lifecycle stages as they produce essentially all components of the

192 oocyst [21, 41] and this was evident in their production of fluorescent protein. We observed a
193 robust increase in cytosolic mScarlet fluorescence beginning at 8 hours (Fig 2K), this fluorescence
194 reached peak intensity 12-14 hours after invasion (note that we did not correct for photobleaching
195 and that fluorescence thus diminishes in the absence of new synthesis). We note that both these
196 timeframes are match the time to egress for male gametes. Interestingly, all three parasite stages
197 are morphologically indistinguishable for the first 6-8 hours after invasion, after which male and
198 asexual parasites begin to divide their nuclei, while female parasites continue to increase in size
199 (S3 Fig).
200
201 **Long term imaging reveals three generations of meronts followed by gametes**
202 Our imaging covered a total of 60 hours of parasite development in multiple overlapping
203 experiments. We tracked hundreds of individual parasites and mapped them onto the overall
204 lifecycle timeline. Figure 3A shows each cell as a line, with the start representing invasion, and
205 the end showing the time of egress (egress is only shown for meronts (green) and male gametes
206 (blue) as female parasites do not egress). We next mapped all observed nuclear divisions, as well
207 as invasion and egress events as individual time points (Fig 3 B-E). These analyses revealed
208 three waves of merogony followed by a single wave of gamete development (please note that we
209 only observed the tail end of the first wave as we start imaging at 11 hours). Waves begin with a
210 relatively sharp line followed by a trail of ‘late comers’. We note a consistent shift to gametes at
211 40 hours in line with previous studies using immunofluorescence assays [21, 42, 43].
212
213 **Meronts release merozoites committed to either asexual or sexual fate**
214 Next, we searched our image dataset for instances in which we could track successive
215 generations of parasite development. Figure 4A shows selected frames over 27 hours of a time
216 lapse movie (Movie S4). The fate of mature cells is indicated by a colored arrowhead, newly

217 invaded next generation stages are highlighted by white arrowheads. We used this information to
218 derive trees mapping the fate of each parasite cell (Fig 4B shows examples with the interpretation
219 of the cells shown in Fig 4A in the middle). Note that we cannot unambiguously map the origin or
220 fate of all parasites. Merozoites left the field of view, cells were lost due to egress and/or cell
221 death, the simultaneous egress of multiple meronts obscured origin, or phototoxicity stalled the
222 development of some parasites before we could assign fate. Nonetheless, we were able to track
223 the fate of the progeny of 49 meronts. During earlier time points, all merozoites emerging from a
224 meront again gave rise to asexual meronts in the next generation (Fig 4C). As the cultures shifted
225 from their asexual to their sexual phase at 40 hours, we found all progeny of individual meronts
226 to give rise to sexual stages. Importantly, when tracking the offspring of individual meronts, we
227 never observed both asexual and sexual stages developing from the same parental meront. We
228 conclude that merozoites are collectively committed to lifecycle transition which suggests that
229 commitment is most likely to occur during the intracellular development of the meront.
230
231 **Meronts committed to sexual development give rise to both male and female gametes**
232 While merozoites from a single meront were strictly committed to either asexual or sexual
233 fate, they were not collectively committed to a single specific sex. We observed both male and
234 female offspring from the same meront (Fig 4C). Out of 26 individual meronts committed to sexual
235 fate for which we were able to observe the development of at least 2 offspring, we observed both
236 male and female offspring 19 times. We were never able to observe all 8 progeny from any
237 meront, the maximum number of observed offspring was 6, in which 2 developed into males and
238 4 became female. To determine the male to female ratio of offspring from a single meront, we
239 conducted a weighted confidence interval based on all 73 observed offspring from the 26 sexually
240 committed meronts. Based on our observations, the 95% confidence interval suggested that out

of the 8 progeny in each meront, between 1.92 and 3.11 will be male. This is consistent with the fact that we never observed more than 2 male progeny from a single meront.

Gametes develop directly from type I meronts, type II meronts are not apparent

Currently many lifecycles of *Cryptosporidium* depict a morphologically distinct tetraploid generation of asexual parasites called the type II meront, as an intermediate between asexual meronts and gametes (see e.g. the widely reproduced lifecycle from the Centers of Disease Control and Prevention at https://www.cdc.gov/parasites/crypto/pathogen.html). Type II meronts are shown to give rise to four merozoites in contrast to asexual type I meronts which produce eight. This model predicts sexual differentiation to be preceded by a wave of tetraploid meronts (Fig 5A), surprisingly, we did not observe this in a previous study that used molecular markers to define stages [21]. Our live-cell imaging experiments used a nuclear marker that clearly distinguished 4 and 8 nuclei stages and thus provided the opportunity to test this rigorously using a large dataset. We analyzed the eventual fate of 1095 parasites that reached the 4N stage across the 60 hours observed. Parasites were binned by the time at which four nuclei were observed, and then categorized into one of three outcomes (Fig 5B): 1) Disappearance after the 4N stage consistent with egress predicted by type II merogony, 2) progression to 8N prior to egress (predicted by type I merogony), or 3) progression to 16N prior to egress (male gamogony). Parasites that remained 4N until the end of the imaging experiment were excluded from analysis. From 11-40 hours post infection, the vast majority of parasites that reach the 4N stage continued past that stage to the 8N stage prior to egress. During this time, we did not observe male (16N) parasites. After 40.5 hours in culture, the proportion of the population that egresses at the 8N stage decreased markedly over time, while the proportion of the population that develop into males increased at the same rate. Parasites with apparent egress at the 4N stage were rare and importantly, their frequency did not change over the culture time and lifecycle.

Loss of fluorescence, used here as a proxy for egress, is indistinguishable from host cell death or lysis due to the egress of another parasite in cells carrying multiple infections. We thus sought to independently evaluate whether 4N meronts do or do not produce merozoites and egress using molecular markers. Apicomplexan parasites assemble the organelles required for invasion at the very end of the cell cycle, and in those parasites replicating by schizogony, rhoptries and micronemes are only apparent in formed merozoite immediately preceding egress [37, 44]. Several rhoptry bulb proteins were recently described for *C. parvum*, and their expression was found to be similarly restricted to parasites harboring merozoites poised to egress [36]. We evaluated two time points (20 and 34 hours) to observe meronts committed to asexual or sexual fate in the next generation, respectively and scored the expression of ROP3-HA in 4N and 8N parasites by immunofluorescence. Labeling was exclusively found in 8N parasites regardless of the point in the progression of the lifecycle they were observed (Fig 5D and G).

Key transitions in the intracellular development of apicomplexan parasites are regulated by the activity of calcium dependent kinases (CDPKs) [45]. CDPK1, an important drug target in *C. parvum* [46], was recently shown to underly strict cell cycle regulation. The protein was only detectable in late stages prior to egress and in very young stages following invasion [47]. We scored the presence of CDPK1-HA in 4N and 8N parasites by immunofluorescence at 20 and 34 hours. CDPK1 staining was only found in 8N stages (Fig 5E), and quantification showed this to be highly reproducible (Fig 5H). We considered that there might be differences between parasite development in vitro and in vivo and thus infected mice with CDPK1-HA parasites. Mice were sacrificed at the peak of infection, small intestines were resected, fixed, frozen and sectioned (see Material and Methods for detail). Cryo-sections of the tissue were incubated with antibodies to HA, lactate dehydrogenase (a marker of all parasite stages), and Hoechst to label DNA. We identified a total of 159 CDPK1 positive cells in 26 fields of view for which we then scored the

number of nuclei in the Hoechst channel. All positive cells have a single or eight nuclei and again we did not detect CDPK1 in 4N parasites (Fig. 5F). Taken together, our culture and animal studies find no evidence for a tetraploid type II meront stage, and we conclude that development to gametes occurs directly from meronts that produce eight merozoites. Importantly, we directly observed this transition (e.g. 4A and B) in our time lapse experiments 26 times.

Discussion

Apicomplexa undergo a cascade of developmental changes as they transition through their lifecycles. More than a century of investigation described a complex succession of morphological types that are specifically adapted to the tasks of invasion and intracellular replication in different hosts, organs, and tissues. This includes specialized transmission stages that carry the infection from one host to the next. As these are single celled organisms, differentiation is not terminal or rigidly inherited, but rather a continuous flow in which each generation elaborates a transient fate. Edward Tyzzer in his initial description of the *Cryptosporidium muris* lifecycle identified three intracellular stages: microgamonts that produced 16 microgametes, macrogamonts that produced single macrogametes, and asexual schizonts. He commented that “the number of merozoites produced in this process of schizogony is almost invariably eight” [48] he also described fertilization and oocyst formation resulting in parasite stages containing four sporozoites. The concept of the tetraploid type II meront as a developmental intermediate between the asexual and sexual reproduction was introduced by John Vetterling in 1971 [49, 50] in studies on *C. wraii* a parasite of guinea pigs. This might have been inspired by his extensive work on *Eimeria* in various animals where distinct meront types occur [51, 52]. At the time *Cryptosporidium* and *Eimeria* were seen as closely related members of the Coccidia (a phylogenetic view no longer held [53, 54]). Vetterling’s two meront model has been cited widely since [55] and has become the text book lifecycle for *Cryptosporidium*. The core of the argument between these authors was how to

316 interpret the tetraploid intracellular parasites found in infected animals and cultures. Are they
317 mature meronts that will yield four merozoites committed to sexual differentiation, or are these
318 immature stages that will undergo further nuclear divisions or form oocysts? This was difficult to
319 resolve using fixed samples, and we therefore chose to study living cells. We documented the
320 fate of more than a thousand tetraploid parasites by time-lapse microcopy and our observations
321 are entirely consistent with Tyzzer's original assertion that all meronts produce eight merozoites
322 – we find no evidence for a type II meront. Molecular markers that report on parasite cell cycle
323 progression further support this in culture and in infected animals. We note that we have not tested
324 *C. wrai*, the guineapig parasite Vetterling used in his original work, however, for *C. parvum*, the
325 most widely studied species of this parasite genus we demonstrate a simple and direct lifecycle
326 of only three morphologically distinct intracellular stages: meronts that yield eight merozoites,
327 male gamonts, and female gametes (Fig. 6A).
328
329 The intracellular development of *Cryptosporidium* appears modular. For the initial eight
330 hours all intracellular stages regardless of their eventual fate are morphologically
331 indistinguishable. We discern a uniform phase establishing the intracellular reproductive niche
332 that is associated with initial growth and biomass increase. The parasites inject host modulating
333 factors that likely play a role in establishing their replicative niche during and following invasion
334 [36, 56]. Establishment of a protein export system is required for the delivery of the parasite protein
335 MEDLE2 to the host cytosol. This takes about five hours to become operational and is active in
336 both asexual and sexual stages. Following the initial establishment phase, the cellular programs
337 diverge markedly leading to asexual merozoites, or male and female gametes. This process is
338 highly synchronous yielding a stage specific number of progeny, over a similar roughly 12 hour
339 time frame (eight merozoites, 16 male gametes, and a single female gamete). This is fast when
340 compared to other apicomplexans where intracellular cycles unfold over days, and may represent

an adaptation to the intestinal epithelium with its high directional turnover with cells being constantly shed at the tip of each villus.

A striking feature of *C. parvum* development is the dramatic switch from asexual to sexual reproduction following three generations of meronts, with gametes discernable at 48 hours [21, 42, 43]. In our experiments we found no evidence for an environmental sex inducing factor, the parasite adhered to a rigid timetable of differentiation in different scenarios of media transfer or coinfection. This suggests an intrinsic developmental program that is reset by sex and is consistent with the link between sex and growth observed by multiple investigators [21-23]. This contrast with *Plasmodium* where transition to sex is sensitive to environmental and metabolic indicators and stressors [27, 28] which is critical to achieving balance between colonization and transmission [57]. To understand how *Cryptosporidium* might be able to forgo such regulation it is important to consider that, in contrast to *Plasmodium*, for this parasite sex is not solely linked to transmission but contributes to continued infection. This may shift the colonization/transmission balance to the oocyst and the likelihood that sporozoites will excyst immediately. The parasite may be able to integrate environmental cues into this step. Interestingly, some authors reported thin shelled and thick shell oocyst that may morphologically reflect the dichotomy of local infection and transmission [40] but experimental confirmation of such a mechanism is still missing.

It is technically difficult to establish whether the parasite adheres to its rigid pattern or timing in animals. However, we believe this to be likely, and note that oocyst shedding is detectable on the third day of infection of mice consistent with the time frame observed in culture [18]. The mechanism underlying this intrinsic lifecycle transition is unknown, the parasite may measure time, the number of intracellular cycles, or the accumulation or depletion of a particular molecule or epigenetic mark. A variety of such mechanisms have been explored in the context of the self-

limiting expansion of stem cell populations [58] and this may stimulate future studies. Among Apicomplexa the transition from asexual to sexual stages has been most intensively studied in *Plasmodium* [59], where the transcription factor AP2-G was shown to be required for gametocyte production [60, 61]. AP2-G acts as a master regulator of sex-specific gene expression through a cascade of transcription factors and additional regulatory genes [61]. AP2-G itself is epigenetically silenced in a Heterochromatin protein1 (HP1) dependent manner during asexual growth [62] and HP1 silencing is removed by the protein gametocyte development 1 (GDV1) [63], which is expressed when *Plasmodium* parasites are grown under conditions that favor sexual stage development. While there are no obvious homologs of HP1 and GDV1 in *Cryptosporidium,* a similar epigenetic switch could nonetheless underlie the sexual commitment that we observed here. Very little is known about epigenetic gene expression regulation in *Cryptosporidium*, beyond that the *C. parvum* genome encodes some histone modification enzymes [64] and that the parasites are susceptible to pharmacological inhibition of these pathways [65, 66]. Future studies analyzing the level of histone modification across the genome and across the lifecycle could reveal such a mechanism.

While sex is an ancient phenomenon found in most eukaryotes, how the specific sex or mating type of individuals is determined is varied and evolutionary malleable [67]. Sex can be inherited, be determined by environmental factors like temperature, or be 'negotiated' between different members of a population by social behavior, biochemical clues, or cell-cell interaction and associated signaling events [68-73]. How sex is determined in Apicomplexa is unknown [31, 74] but sexual differentiation and sex-ratio play important roles in transmission and environmental adaptation [57]. In *Plasmodium* the offspring of individual schizonts is thought to be collectively committed to a male or female fate in a mutually exclusive fashion [75]. One of the most interesting observations of our study in *Cryptosporidium*, however, is that the sexually committed meront

consistently gives rise to both males and females (Fig. 4). We propose that this makes it likely that the future sex of individual merozoites and thus the sex ratio is determined in the meront prior to egress (Fig. 6B). The mechanism by which this is achieved remains to be discovered. The fact that commitment occurs over the backdrop of cell division may inform the discussion and offers hypotheses. Unequal inheritance or asymmetrical segregation of fate determining organelles or molecules is well established in the differentiation of mammalian cells and embryos [76, 77] and could be at play here. We note an abundance of sex-specific non-coding RNAs in *Cryptosporidium* [78] as one set of potential candidates. There is also an emerging understanding of mechanisms that yield differential inheritance of epigenetic histone modification, and this can occur at different steps of DNA synthesis and mitotic segregation [79]. The mechanism could be stochastic instead of directive, it may not matter which specific merozoite adopts a certain fate as long as the desired sex ratio is achieved. Overall, the model predicts merozoite heterogeneity, and experiments that would reveal the molecular nature of such heterogeneity could provide clues as to how sex is determined. An important biological consequence of the *Cryptosporidium* commitment model is that male and female gametes by default will develop in close spatial proximity. Even at very low initial parasite burden this mechanism provides a safe route towards fertilization through selfing. This may be critical for a parasite that relies on a sexual lifecycle reset for continued growth [21-23]. *Cryptosporidium* provides the opportunity to analyze the fundamental molecular tenants of apicomplexan lifecycle progression, sex determination, and gamete interaction in a stripped-down single host lifecycle. In this study, we showed it to unfold in culture and over the course of only four infectious cycles in less than 72 hours, and to employ a minimal cast of three morphological types.

Materials and Methods

Generation of Transgenic Parasites

Transgenic parasites were generated using previously described methods [20, 80]. Briefly, 5 x 10^7 C. parvum oocysts (Iowa II strain obtained from Bunchgrass Farms) were bleached and washed prior to incubation in 0.8% sodium taurocholate for 1 hour at 37 C to induce excystation. Following excystation a CRISPR guide plasmid and repair template with 50 base pair homology arms were introduced via nucleofection using the AMAXA 4D Nucleofector (Lonza). Transfected sporozoites were then diluted in PBS and used to infect a cage of mice. Here we used the modified protocol for infection in which mice were given 100 μL of 8% sodium bicarbonate solution by oral gavage 10 minutes prior to oral gavage with the transfected parasites [80]. Stable transformants were selected with 16 mg/mL paromomycin (in drinking water at libitum) and parasite shedding was monitored via nanoluciferase activity in the feces of infected mice [20].

Transgenic parasites were isolated from feces by sucrose floatation followed by cesium chloride gradient [81] and then stored at 4 C in PBS until used for each experiment.

Immunofluorescence Assay

Human adeno carcinoma HCT-8 (ATTC CCL-244) cells were maintained by serial passage in RPMI-1640 containing 10% fetal bovine serum (FBS). Immediately prior to infection, the medium was exchanged to RPMI-1640 containing 1% FBS. HCT-8 cells were infected with oocysts that were bleached using 10% bleach for 10 minutes at 4 C, washed 3 times with cold PBS, excysted with 0.8% sodium taurocholate at 37 C for 10 minutes, and washed once with PBS before addition to the culture. Infected HCT-8s were fixed using 4% paraformaldehyde for 10 minutes, then washed and permeabilized with 0.25% triton x-100 for 10 minutes. Fixed and permeabilized cells were then blocked with 3% bovine serum albumin (BSA) for 1 hour at room temperature prior to incubation with primary antibodies for 1 hour at room temperature.

For immunohistology, ifng-/- mice (Jackson Laboratories Strain 002287 bred inhouse) were infected with 10,000 CDPK1-HA oocysts (a kind gift of Dr. Sumiti Vinayak, University of Illinois Urbana-Champaign) and their intestines were resected and 'swiss-rolled' prior to fixation overnight in formalin. Cryo-sectioning was performed by the PennVet Pathology core facility and immunofluorescence was performed as described [18].

Antibodies and dye used: anti-HA (Roche clone 3F10), VVL-FITC (Vector FL1231), anti-LDH (a kind gift of Dr. Guan Zhu Texas A&M University, now Jilin University [82]).

Following incubation with primary antibodies, coverslips were washed three times with PBS at room temperature, then incubated with appropriate secondary antibodies in 3% BSA for one hour at room temperature. Cells were counterstained with DAPI or Hoechst for 10 minutes, washed with PBS twice and then mounted on slides with Fluoromount or Vectashield. Coverslips were observed using a Leica DM6000B Upright Widefield Microscope using 63x or 100x objectives or a GE DeltaVision OMX Structured Resolution Microscope using a 60x objective. Both microscopes are maintained by the Penn Vet Imaging Core.

Acquisition and Processing of Live-Imaging Data

8-well chamber slides (Ibidi) were seeded with HCT-8 cells, which were then grown in RPMI-1640 supplemented with 10% FBS at 37 C, 5% CO2 for 24-48 hours prior to infection. Host cells were switch to pre-warmed RPMI-1640 supplemented with 1% FBS immediately prior to infection with bleached, washed and excysted sporozoites. Imaging was preformed beginning at various time points using a GE DeltaVision OMX Structured Resolution Microscope using the conventional light path. Growth conditions were maintained throughout each imaging experiment at 37 C, 5% CO2 and 40-60% humidity. Using the AquireSR Acquisition control software, Z-stacks were taken in both the 488 and 568 channels for multiple points of interest every 30 minutes for up to 42 hours. Images were processed using the softWoRx image reconstruction and analysis

software. Briefly, images were deconvolved, the channels were then aligned, and the z-stacks were compressed to generate a 2-channel image for each time point. Manual drift correction was applied in ImageJ to generate movies and stills of individual developing parasites. Ten independent experiments were performed, we collected a total of 6171 hours of images and were able to analyze 4542.5 hours containing growth and replication information for 1365 individual intracellular parasites.

Analysis of Live-Imaging Data

Analysis was performed using 2-channel time series data obtained as described above. Parasites were manually tracked and recorded for time of invasion, any subsequent nuclear replication events, and apparent egress. Data was graphed and analyzed using GraphPad Prism and Microsoft Excel software.

Statistical Analysis

The weighted confidence interval was performed in Microsoft Excel using the observational data from 73 offspring of 26 sexually committed meronts. All other statistical analyses were performed using GraphPad Prism.

Acknowledgements

This work was supported in part by grant R01AI127798 from the National Institutes of Health to BS and a postdoctoral fellowship from EMBO to AG (ALTF 58-2018). We are grateful to Drs. Vinayak and Zhu for sharing reagents with us and to the PennVet pathology and imaging core for assistance. We would also like to thank members of our laboratory, particularly Dr. Katelyn Walzer for ongoing discussions and feedback.

References

1. Collaborators GBDDD. Estimates of global, regional, and national morbidity, mortality, and aetiologies of diarrhoeal diseases: a systematic analysis for the Global Burden of Disease Study 2015. Lancet Infect Dis. 2017;17(9):909-48. Epub 2017/06/06. doi: 10.1016/S1473-3099(17)30276-1. PubMed PMID: 28579426; PubMed Central PMCID: PMCPMC5589208.

2. Kotloff KL, Nataro JP, Blackwelder WC, Nasrin D, Farag TH, Panchalingam S, et al. Burden and aetiology of diarrhoeal disease in infants and young children in developing countries (the Global Enteric Multicenter Study, GEMS): a prospective, case-control study. Lancet. 2013;382(9888):209-22. Epub 2013/05/18. doi: 10.1016/S0140-6736(13)60844-2. PubMed PMID: 23680352.

3. Checkley W, White AC, Jr., Jaganath D, Arrowood MJ, Chalmers RM, Chen XM, et al. A review of the global burden, novel diagnostics, therapeutics, and vaccine targets for cryptosporidium. Lancet Infect Dis. 2015;15(1):85-94. doi: 10.1016/S1473-3099(14)70772-8. PubMed PMID: 25278220; PubMed Central PMCID: PMCPMC4401121.

4. Mondal D, Minak J, Alam M, Liu Y, Dai J, Korpe P, et al. Contribution of Enteric Infection, Altered Intestinal Barrier Function, and Maternal Malnutrition to Infant Malnutrition in Bangladesh. Clinical Infectious Diseases. 2012;54(2):185-92. doi: 10.1093/cid/cir807. PubMed PMID: WOS:000298383700006.

5. Korpe PS, Petri WA, Jr. Environmental enteropathy: critical implications of a poorly understood condition. Trends Mol Med. 2012;18(6):328-36. doi: 10.1016/j.molmed.2012.04.007. PubMed PMID: 22633998; PubMed Central PMCID: PMCPMC3372657.

6. Khalil IA, Troeger C, Rao PC, Blacker BF, Brown A, Brewer TG, et al. Morbidity, mortality, and long-term consequences associated with diarrhoea from Cryptosporidium infection in children younger than 5 years: a meta-analyses study. Lancet Glob Health. 2018;6(7):e758-e68. Epub 2018/06/16. doi: 10.1016/S2214-109X(18)30283-3. PubMed PMID: 29903377; PubMed Central PMCID: PMCPMC6005120.

7. Kabir M, Alam M, Nayak U, Arju T, Hossain B, Tarannum R, et al. Nonsterile immunity to cryptosporidiosis in infants is associated with mucosal IgA against the sporozoite and protection from malnutrition. PLoS Pathog. 2021;17(6):e1009445. Epub 2021/06/29. doi: 10.1371/journal.ppat.1009445. PubMed PMID: 34181697; PubMed Central PMCID: PMCPMC8270466.

8. Amadi B, Mwiya M, Sianongo S, Payne L, Watuka A, Katubulushi M, et al. High dose prolonged treatment with nitazoxanide is not effective for cryptosporidiosis in HIV positive Zambian children: a

randomised controlled trial. BMC infectious diseases. 2009;9:195. doi: 10.1186/1471-2334-9-195. PubMed PMID: 19954529; PubMed Central PMCID: PMC2794874.

9. Choy RKM, Huston CD. Cryptosporidiosis should be designated as a tropical disease by the US Food and Drug Administration. PLoS neglected tropical diseases. 2020;14(7):e0008252. Epub 2020/07/03. doi: 10.1371/journal.pntd.0008252. PubMed PMID: 32614819; PubMed Central PMCID: PMCPMC7332027 following competing interests: CDH is inventor on a US patent for the use of MMV665917 and triazolopyridazine analogs for treatment and prevention of cryptosporidiosis.

10. Manjunatha UH, Vinayak S, Zambriski JA, Chao AT, Sy T, Noble CG, et al. A Cryptosporidium PI(4)K inhibitor is a drug candidate for cryptosporidiosis. Nature. 2017;546(7658):376-80. doi: 10.1038/nature22337. PubMed PMID: 28562588; PubMed Central PMCID: PMCPMC5473467.

11. Baragana B, Forte B, Choi R, Hewitt SN, Bueren-Calabuig JA, Pisco JP, et al. Lysyl-tRNA synthetase as a drug target in malaria and cryptosporidiosis. P Natl Acad Sci USA. 2019;116(14):7015-20. doi: 10.1073/pnas.1814685116. PubMed PMID: WOS:000463069900080.

12. Bessoff K, Sateriale A, Lee KK, Huston CD. Drug repurposing screen reveals FDA-approved inhibitors of human HMG-CoA reductase and isoprenoid synthesis that block Cryptosporidium parvum growth. Antimicrob Agents Chemother. 2013;57(4):1804-14. Epub 2013/02/06. doi: 10.1128/AAC.02460-12. PubMed PMID: 23380723; PubMed Central PMCID: PMC3623326.

13. Jumani RS, Bessoff K, Love MS, Miller P, Stebbins EE, Teixeira JE, et al. A Novel Piperazine-Based Drug Lead for Cryptosporidiosis from the Medicines for Malaria Venture Open-Access Malaria Box. Antimicrob Agents Chemother. 2018;62(4). doi: 10.1128/AAC.01505-17. PubMed PMID: 29339392; PubMed Central PMCID: PMCPMC5913971.

14. Vinayak S, Jumani RS, Miller P, Hasan MM, McLeod BI, Tandel J, et al. Bicyclic azetidines kill the diarrheal pathogen Cryptosporidium in mice by inhibiting parasite phenylalanyl-tRNA synthetase. Sci Transl Med. 2020;12(563). Epub 2020/10/02. doi: 10.1126/scitranslmed.aba8412. PubMed PMID: 32998973; PubMed Central PMCID: PMCPMC8381743.

15. Love MS, Beasley FC, Jumani RS, Wright TM, Chatterjee AK, Huston CD, et al. A high-throughput phenotypic screen identifies clofazimine as a potential treatment for cryptosporidiosis. PLoS neglected tropical diseases. 2017;11(2):e0005373. doi: 10.1371/journal.pntd.0005373. PubMed PMID: 28158186; PubMed Central PMCID: PMCPMC5310922.

549 16. Flannery EL, Chatterjee AK, Winzeler EA. Antimalarial drug discovery - approaches and progress
550 towards new medicines. Nat Rev Microbiol. 2017;15(9):572. Epub 2017/07/25. doi:
551 10.1038/nrmicro.2017.88. PubMed PMID: 28736448.
552 17. Sateriale A, Slapeta J, Baptista R, Engiles JB, Gullicksrud JA, Herbert GT, et al. A Genetically
553 Tractable, Natural Mouse Model of Cryptosporidiosis Offers Insights into Host Protective Immunity. Cell
554 Host Microbe. 2019;26(1):135-46 e5. Epub 2019/06/25. doi: 10.1016/j.chom.2019.05.006. PubMed PMID:
555 31231045; PubMed Central PMCID: PMCPMC6617386.
556 18. Gullicksrud JA, Sateriale A, Engiles JB, Gibson AR, Shaw S, Hutchins ZA, et al. Enterocyte-innate
557 lymphoid cell crosstalk drives early IFN-gamma-mediated control of Cryptosporidium. Mucosal Immunol.
558 2021. Epub 2021/11/10. doi: 10.1038/s41385-021-00468-6. PubMed PMID: 34750455.
559 19. Griffiths JK, Theodos C, Paris M, Tzipori S. The gamma interferon gene knockout mouse: a highly
560 sensitive model for evaluation of therapeutic agents against Cryptosporidium parvum. J Clin Microbiol.
561 1998;36(9):2503-8. PubMed PMID: 9705383.
562 20. Vinayak S, Pawlowic MC, Sateriale A, Brooks CF, Studstill CJ, Bar-Peled Y, et al. Genetic modification
563 of the diarrhoeal pathogen Cryptosporidium parvum. Nature. 2015;523(7561):477-80. Epub 2015/07/16.
564 doi: 10.1038/nature14651. PubMed PMID: 26176919; PubMed Central PMCID: PMCPMC4640681.
565 21. Tandel J, English ED, Sateriale A, Gullicksrud JA, Beiting DP, Sullivan MC, et al. Life cycle progression
566 and sexual development of the apicomplexan parasite Cryptosporidium parvum. Nat Microbiol.
567 2019;4(12):2226-36. Epub 2019/09/04. doi: 10.1038/s41564-019-0539-x. PubMed PMID: 31477896;
568 PubMed Central PMCID: PMCPMC6877471.
569 22. Heo I, Dutta D, Schaefer DA, Iakobachvili N, Artegiani B, Sachs N, et al. Modelling Cryptosporidium
570 infection in human small intestinal and lung organoids. Nat Microbiol. 2018;3(7):814-+. doi:
571 10.1038/s41564-018-0177-8. PubMed PMID: WOS:000436530900010.
572 23. Wilke G, Funkhouser-Jones LJ, Wang Y, Ravindran S, Wang Q, Beatty WL, et al. A Stem-Cell-Derived
573 Platform Enables Complete Cryptosporidium Development In Vitro and Genetic Tractability. Cell Host
574 Microbe. 2019;26(1):123-34 e8. doi: 10.1016/j.chom.2019.05.007. PubMed PMID: 31231046; PubMed
575 Central PMCID: PMCPMC6617391.
576 24. Nikolaev M, Mitrofanova O, Broguiere N, Geraldo S, Dutta D, Tabata Y, et al. Homeostatic mini-
577 intestines through scaffold-guided organoid morphogenesis. Nature. 2020;585(7826):574-+. doi:
578 10.1038/s41586-020-2724-8. PubMed PMID: WOS:000570130400002.

579 25. Smalley ME, Brown J, Bassett NM. The rate of production of Plasmodium falciparum gametocytes
580 during natural infections. Transactions of the Royal Society of Tropical Medicine and Hygiene.
581 1981;75(2):318-9. Epub 1981/01/01. doi: 10.1016/0035-9203(81)90349-7. PubMed PMID: 7029806.
582 26. Kuehn A, Pradel G. The coming-out of malaria gametocytes. J Biomed Biotechnol.
583 2010;2010:976827. Epub 2010/01/30. doi: 10.1155/2010/976827. PubMed PMID: 20111746; PubMed
584 Central PMCID: PMCPMC2810480.
585 27. Brancucci NMB, Gerdt JP, Wang C, De Niz M, Philip N, Adapa SR, et al. Lysophosphatidylcholine
586 Regulates Sexual Stage Differentiation in the Human Malaria Parasite Plasmodium falciparum. Cell.
587 2017;171(7):1532-44 e15. Epub 2017/11/14. doi: 10.1016/j.cell.2017.10.020. PubMed PMID: 29129376;
588 PubMed Central PMCID: PMCPMC5733390.
589 28. Venugopal K, Hentzschel F, Valkiunas G, Marti M. Plasmodium asexual growth and sexual
590 development in the haematopoietic niche of the host. Nat Rev Microbiol. 2020;18(3):177-89. Epub
591 2020/01/11. doi: 10.1038/s41579-019-0306-2. PubMed PMID: 31919479; PubMed Central PMCID:
592 PMCPMC7223625.
593 29. Sokol-Borrelli SL, Coombs RS, Boyle JP. A Comparison of Stage Conversion in the Coccidian
594 Apicomplexans Toxoplasma gondii, Hammondia hammondi, and Neospora caninum. Front Cell Infect
595 Microbiol. 2020;10:608283. Epub 2020/12/22. doi: 10.3389/fcimb.2020.608283. PubMed PMID:
596 33344268; PubMed Central PMCID: PMCPMC7744739.
597 30. Sokol SL, Primack AS, Nair SC, Wong ZS, Tembo M, Verma SK, et al. Dissection of the in vitro
598 developmental program of Hammondia hammondi reveals a link between stress sensitivity and life cycle
599 flexibility in Toxoplasma gondii. Elife. 2018;7. Epub 2018/05/23. doi: 10.7554/eLife.36491. PubMed PMID:
600 29785929; PubMed Central PMCID: PMCPMC5963921.
601 31. Walker RA, Ferguson DJ, Miller CM, Smith NC. Sex and Eimeria: a molecular perspective.
602 Parasitology. 2013;140(14):1701-17. doi: 10.1017/S0031182013000838. PubMed PMID: 23953058.
603 32. McDonald V, Rose ME. Eimeria tenella and E. necatrix: a third generation of schizogony is an
604 obligatory part of the developmental cycle. J Parasitol. 1987;73(3):617-22. Epub 1987/06/01. PubMed
605 PMID: 3598808.
606 33. Soete M, Camus D, Dubremetz JF. Experimental induction of bradyzoite-specific antigen expression
607 and cyst formation by the RH strain of Toxoplasma gondii in vitro. Exp Parasitol. 1994;78(4):361-70.

608 34. Fox BA, Gigley JP, Bzik DJ. Toxoplasma gondii lacks the enzymes required for de novo arginine
609 biosynthesis and arginine starvation triggers cyst formation. Int J Parasitol. 2004;34(3):323-31. Epub
610 2004/03/09. doi: 10.1016/j.ijpara.2003.12.001. PubMed PMID: 15003493.
611 35. Rojas F, Silvester E, Young J, Milne R, Tettey M, Houston DR, et al. Oligopeptide Signaling through
612 TbGPR89 Drives Trypanosome Quorum Sensing. Cell. 2019;176(1-2):306-17 e16. Epub 2018/12/07. doi:
613 10.1016/j.cell.2018.10.041. PubMed PMID: 30503212; PubMed Central PMCID: PMCPMC6333907.
614 36. Guerin A, Roy NH, Kugler EM, Berry L, Burkhardt JK, Shin JB, et al. Cryptosporidium rhoptry effector
615 protein ROP1 injected during invasion targets the host cytoskeletal modulator LMO7. Cell Host Microbe.
616 2021;29(9):1407-20 e5. Epub 2021/08/05. doi: 10.1016/j.chom.2021.07.002. PubMed PMID: 34348092;
617 PubMed Central PMCID: PMCPMC8475647.
618 37. Francia ME, Striepen B. Cell division in apicomplexan parasites. Nat Rev Microbiol. 2014;12(2):125-
619 36. doi: 10.1038/nrmicro3184. PubMed PMID: 24384598.
620 38. Arnot DE, Ronander E, Bengtsson DC. The progression of the intra-erythrocytic cell cycle of
621 Plasmodium falciparum and the role of the centriolar plaques in asynchronous mitotic division during
622 schizogony. Int J Parasitol. 2011;41(1):71-80. Epub 2010/09/08. doi: 10.1016/j.ijpara.2010.07.012.
623 PubMed PMID: 20816844.
624 39. Ostrovska K, Paperna I. Cryptosporidium sp. of the starred lizard Agame stellio:ultrastructure and
625 life cycle. Parasitology Research. 1990;76:712-20.
626 40. Cheadle MA, Toivio-Kinnucan M, Blagburn BL. The ultrastructure of gametogenesis of
627 cryptosporidium baileyi (eimeriorina; cryptosporidiidae) in the respiratory tract of broiler chickens (Gallus
628 domesticus). J Parasitol. 1999;85(4):609-15. Epub 1999/08/26. PubMed PMID: 10461939.
629 41. Templeton TJ, Lancto CA, Vigdorovich V, Liu C, London NR, Hadsall KZ, et al. The Cryptosporidium
630 oocyst wall protein is a member of a multigene family and has a homolog in Toxoplasma. Infection and
631 Immunity. 2004;72(2):980-7. doi: 10.1128/Iai.72.2.980-987.2004. PubMed PMID:
632 WOS:000188766400044.
633 42. Jumani RS, Hasan MM, Stebbins EE, Donnelly L, Miller P, Klopfer C, et al. A suite of phenotypic
634 assays to ensure pipeline diversity when prioritizing drug-like Cryptosporidium growth inhibitors. Nature
635 communications. 2019;10(1):1862. doi: 10.1038/s41467-019-09880-w. PubMed PMID: 31015448;
636 PubMed Central PMCID: PMCPMC6478823.
637 43. Wilke G, Ravindran S, Funkhouser-Jones L, Barks J, Wang Q, VanDussen KL, et al. Monoclonal
638 Antibodies to Intracellular Stages of Cryptosporidium parvum Define Life Cycle Progression In Vitro.

639 mSphere. 2018;3(3). doi: 10.1128/mSphere.00124-18. PubMed PMID: 29848759; PubMed Central PMCID:
640 PMCPMC5976880.
641 44. Counihan NA, Kalanon M, Coppel RL, de Koning-Ward TF. Plasmodium rhoptry proteins: why order
642 is important. Trends Parasitol. 2013;29(5):228-36. Epub 2013/04/11. doi: 10.1016/j.pt.2013.03.003.
643 PubMed PMID: 23570755.
644 45. Lourido S, Moreno SN. The calcium signaling toolkit of the Apicomplexan parasites Toxoplasma
645 gondii and Plasmodium spp. Cell Calcium. 2015;57(3):186-93. Epub 2015/01/22. doi:
646 10.1016/j.ceca.2014.12.010. PubMed PMID: 25605521; PubMed Central PMCID: PMCPMC4428288.
647 46. Hulverson MA, Vinayak S, Choi R, Schaefer DA, Castellanos-Gonzalez A, Vidadala RSR, et al.
648 Bumped-Kinase Inhibitors for Cryptosporidiosis Therapy. J Infect Dis. 2017;215(8):1275-84. Epub
649 2017/03/23. doi: 10.1093/infdis/jix120. PubMed PMID: 28329187; PubMed Central PMCID:
650 PMCPMC5853794.
651 47. Choudhary HH, Nava MG, Gartlan BE, Rose S, Vinayak S. A Conditional Protein Degradation System
652 To Study Essential Gene Function in Cryptosporidium parvum. mBio. 2020;11(4). Epub 2020/08/28. doi:
653 10.1128/mBio.01231-20. PubMed PMID: 32843543; PubMed Central PMCID: PMCPMC7448269.
654 48. Tyzzer EE. An extracellular Coccidium, Cryptosporidium Muris (Gen. Et Sp. Nov.), of the gastric
655 Glands of the Common Mouse. J Med Res. 1910;23(3):487-510 3. PubMed PMID: 19971982; PubMed
656 Central PMCID: PMCPMC2098948.
657 49. Vetterling JM, Jervis HR, Merrill TG, Sprinz H. Cryptosporidium wrairi sp. n. from the guinea pig
658 Cavia porcellus, with an emendation of the genus. J Protozool. 1971;18(2):243-7. Epub 1971/05/01. doi:
659 10.1111/j.1550-7408.1971.tb03315.x. PubMed PMID: 4997038.
660 50. Vetterling JM, Takeuchi A, Madden PA. Ultrastructure of Cryptosporidium wrairi from the guinea
661 pig. J Protozool. 1971;18(2):248-60. Epub 1971/05/01. doi: 10.1111/j.1550-7408.1971.tb03316.x.
662 PubMed PMID: 4997039.
663 51. Dubremetz JF. [Genesis of merozoites in the coccidia, Eimeria necatrix. Ultrastructural study]. J
664 Protozool. 1975;22(1):71-84. PubMed PMID: 1117438.
665 52. Muller BE. Ultrastructural development of first- to second-generation merozoites in Eimeria
666 contorta Haberkorn, 1971. Z Parasitenkd. 1975;47(2):91-101.
667 53. Carreno RA, Martin DS, Barta JR. Cryptosporidium is more closely related to the gregarines than to
668 coccidia as shown by phylogenetic analysis of apicomplexan parasites inferred using small-subunit
669 ribosomal RNA gene sequences. Parasitol Res. 1999;85(11):899-904. PubMed PMID: 10540950.

670 54. Leander BS, Clopton RE, Keeling PJ. Phylogeny of gregarines (Apicomplexa) as inferred from small-
671 subunit rDNA and beta-tubulin. Int J Syst Evol Microbiol. 2003;53(Pt 1):345-54. PubMed PMID: 12656194.
672 55. Current WL, Reese NC. A comparison of endogenous development of three isolates of
673 Cryptosporidium in suckling mice. J Protozool. 1986;33(1):98-108. PubMed PMID: 3959014.
674 56. Dumaine JE, Sateriale A, Gibson AR, Reddy AG, Gullicksrud JA, Hunter E, et al. The enteric pathogen
675 Cryptosporidium parvum exports proteins into the cytosol of the infected cell. Elife. 2021:in press.
676 57. Schneider P, Reece SE. The private life of malaria parasites: Strategies for sexual reproduction. Mol
677 Biochem Parasitol. 2021;244:111375. Epub 2021/05/24. doi: 10.1016/j.molbiopara.2021.111375.
678 PubMed PMID: 34023299; PubMed Central PMCID: PMCPMC8346949.
679 58. Bernitz JM, Kim HS, MacArthur B, Sieburg H, Moore K. Hematopoietic Stem Cells Count and
680 Remember Self-Renewal Divisions. Cell. 2016;167(5):1296-309 e10. Epub 2016/11/15. doi:
681 10.1016/j.cell.2016.10.022. PubMed PMID: 27839867; PubMed Central PMCID: PMCPMC5115957.
682 59. Josling GA, Williamson KC, Llinas M. Regulation of Sexual Commitment and Gametocytogenesis in
683 Malaria Parasites. Annu Rev Microbiol. 2018;72:501-19. Epub 2018/07/06. doi: 10.1146/annurev-micro-
684 090817-062712. PubMed PMID: 29975590; PubMed Central PMCID: PMCPMC7164540.
685 60. Kafsack BF, Rovira-Graells N, Clark TG, Bancells C, Crowley VM, Campino SG, et al. A transcriptional
686 switch underlies commitment to sexual development in malaria parasites. Nature. 2014;507(7491):248-
687 52. doi: 10.1038/nature12920. PubMed PMID: 24572369; PubMed Central PMCID: PMCPMC4040541.
688 61. Sinha A, Hughes KR, Modrzynska KK, Otto TD, Pfander C, Dickens NJ, et al. A cascade of DNA-
689 binding proteins for sexual commitment and development in Plasmodium. Nature. 2014;507(7491):253-
690 7. doi: 10.1038/nature12970. PubMed PMID: 24572359; PubMed Central PMCID: PMCPMC4105895.
691 62. Brancucci NMB, Bertschi NL, Zhu L, Niederwieser I, Chin WH, Wampfler R, et al. Heterochromatin
692 protein 1 secures survival and transmission of malaria parasites. Cell Host Microbe. 2014;16(2):165-76.
693 Epub 2014/08/15. doi: 10.1016/j.chom.2014.07.004. PubMed PMID: 25121746.
694 63. Filarsky M, Fraschka SA, Niederwieser I, Brancucci NMB, Carrington E, Carrio E, et al. GDV1 induces
695 sexual commitment of malaria parasites by antagonizing HP1-dependent gene silencing. Science.
696 2018;359(6381):1259-63. Epub 2018/03/29. doi: 10.1126/science.aan6042. PubMed PMID: 29590075;
697 PubMed Central PMCID: PMCPMC6219702.
698 64. Rider SD, Jr., Zhu G. An apicomplexan ankyrin-repeat histone deacetylase with relatives in
699 photosynthetic eukaryotes. Int J Parasitol. 2009;39(7):747-54. Epub 2009/01/13. doi:
700 10.1016/j.ijpara.2008.11.012. PubMed PMID: 19136004; PubMed Central PMCID: PMCPMC4616004.

65. Guo F, Zhang H, McNair NN, Mead JR, Zhu G. The Existing Drug Vorinostat as a New Lead Against Cryptosporidiosis by Targeting the Parasite Histone Deacetylases. J Infect Dis. 2018;217(7):1110-7. Epub 2018/01/05. doi: 10.1093/infdis/jix689. PubMed PMID: 29300993; PubMed Central PMCID: PMCPMC5939870.

66. Murakoshi F, Bando H, Sugi T, Adeyemi OS, Nonaka M, Nakaya T, et al. Nullscript inhibits Cryptosporidium and Toxoplasma growth. International journal for parasitology Drugs and drug resistance. 2020;14:159-66. Epub 2020/10/30. doi: 10.1016/j.ijpddr.2020.10.004. PubMed PMID: 33120250; PubMed Central PMCID: PMCPMC7593347.

67. Bachtrog D, Mank JE, Peichel CL, Kirkpatrick M, Otto SP, Ashman TL, et al. Sex Determination: Why So Many Ways of Doing It? Plos Biology. 2014;12(7). doi: ARTN e1001899 10.1371/journal.pbio.1001899. PubMed PMID: WOS:000340550400003.

68. Buston P. Social hierarchies: size and growth modification in clownfish. Nature. 2003;424(6945):145-6. Epub 2003/07/11. doi: 10.1038/424145a. PubMed PMID: 12853944.

69. Orias E, Singh DP, Meyer E. Genetics and Epigenetics of Mating Type Determination in Paramecium and Tetrahymena. Annual Review of Microbiology, Vol 71. 2017;71:133-56. doi: 10.1146/annurev-micro-090816-093342. PubMed PMID: WOS:000411800600009.

70. Frenkel J, Vyverman W, Pohnert G. Pheromone signaling during sexual reproduction in algae. Plant J. 2014;79(4):632-44. doi: 10.1111/tpj.12496. PubMed PMID: 24597605.

71. Mori T, Kawai-Toyooka H, Igawa T, Nozaki H. Gamete Dialogs in Green Lineages. Mol Plant. 2015;8(10):1442-54. doi: 10.1016/j.molp.2015.06.008. PubMed PMID: 26145252.

72. Hansson A, Olsson M. Incubation temperature and parental identity determine sex in the Australian agamid lizard Ctenophorus pictus. Ecol Evol. 2018;8(19):9827-33. doi: 10.1002/ece3.4466. PubMed PMID: 30386578; PubMed Central PMCID: PMCPMC6202699.

73. Whiteley SL, Weisbecker V, Georges A, Gauthier ARG, Whitehead DL, Holleley CE. Developmental asynchrony and antagonism of sex determination pathways in a lizard with temperature-induced sex reversal. Scientific reports. 2018;8(1):14892. doi: 10.1038/s41598-018-33170-y. PubMed PMID: 30291276; PubMed Central PMCID: PMCPMC6173690.

74. Smith TG, Walliker D, Ranford-Cartwright LC. Sexual differentiation and sex determination in the Apicomplexa. Trends Parasitol. 2002;18(7):315-23. PubMed PMID: 12379952.

730 75. Silvestrini F, Alano P, Williams JL. Commitment to the production of male and female gametocytes
731 in the human malaria parasite Plasmodium falciparum. Parasitology. 2000;121 Pt 5:465-71. Epub
732 2000/12/29. doi: 10.1017/s0031182099006691. PubMed PMID: 11128797.
733 76. Chang JT, Palanivel VR, Kinjyo I, Schambach F, Intlekofer AM, Banerjee A, et al. Asymmetric T
734 lymphocyte division in the initiation of adaptive immune responses. Science. 2007;315(5819):1687-91.
735 Epub 2007/03/03. doi: 10.1126/science.1139393. PubMed PMID: 17332376.
736 77. Salle J, Minc N. Cell division geometries as central organizers of early embryo development. Semin
737 Cell Dev Biol. 2021;in press. Available at https://doi.org/10.1016/j.semcdb.2021.08.004. doi:
738 https://doi.org/10.1016/j.semcdb.2021.08.004.
739 78. Li Y, Baptista RP, Sateriale A, Striepen B, Kissinger JC. Analysis of Long Non-Coding RNA in
740 Cryptosporidium parvum Reveals Significant Stage-Specific Antisense Transcription. Front Cell Infect Mi.
741 2021;10(833). doi: 10.3389/fcimb.2020.608298.
742 79. Xie J, Wooten M, Tran V, Chen X. Breaking Symmetry - Asymmetric Histone Inheritance in Stem
743 Cells. Trends Cell Biol. 2017;27(7):527-40. Epub 2017/03/08. doi: 10.1016/j.tcb.2017.02.001. PubMed
744 PMID: 28268050; PubMed Central PMCID: PMCPMC5476491.
745 80. Sateriale A, Pawlowic M, Vinayak S, Brooks C, Striepen B. Genetic Manipulation of Cryptosporidium
746 parvum with CRISPR/Cas9. Methods Mol Biol. 2020;2052:219-28. Epub 2019/08/28. doi: 10.1007/978-1-
747 4939-9748-0_13. PubMed PMID: 31452165.
748 81. Pawlowic MC, Vinayak S, Sateriale A, Brooks CF, Striepen B. Generating and Maintaining Transgenic
749 Cryptosporidium parvum Parasites. Curr Protoc Microbiol. 2017;46:20B 2 1-B 2 32. doi: 10.1002/cpmc.33.
750 PubMed PMID: 28800157; PubMed Central PMCID: PMCPMC5556942.
751 82. Zhang H, Guo F, Zhu G. Cryptosporidium Lactate Dehydrogenase Is Associated with the
752 Parasitophorous Vacuole Membrane and Is a Potential Target for Developing Therapeutics. PLoS Pathog.
753 2015;11(11):e1005250. Epub 2015/11/13. doi: 10.1371/journal.ppat.1005250. PubMed PMID: 26562790;
754 PubMed Central PMCID: PMCPMC4642935.
755
756

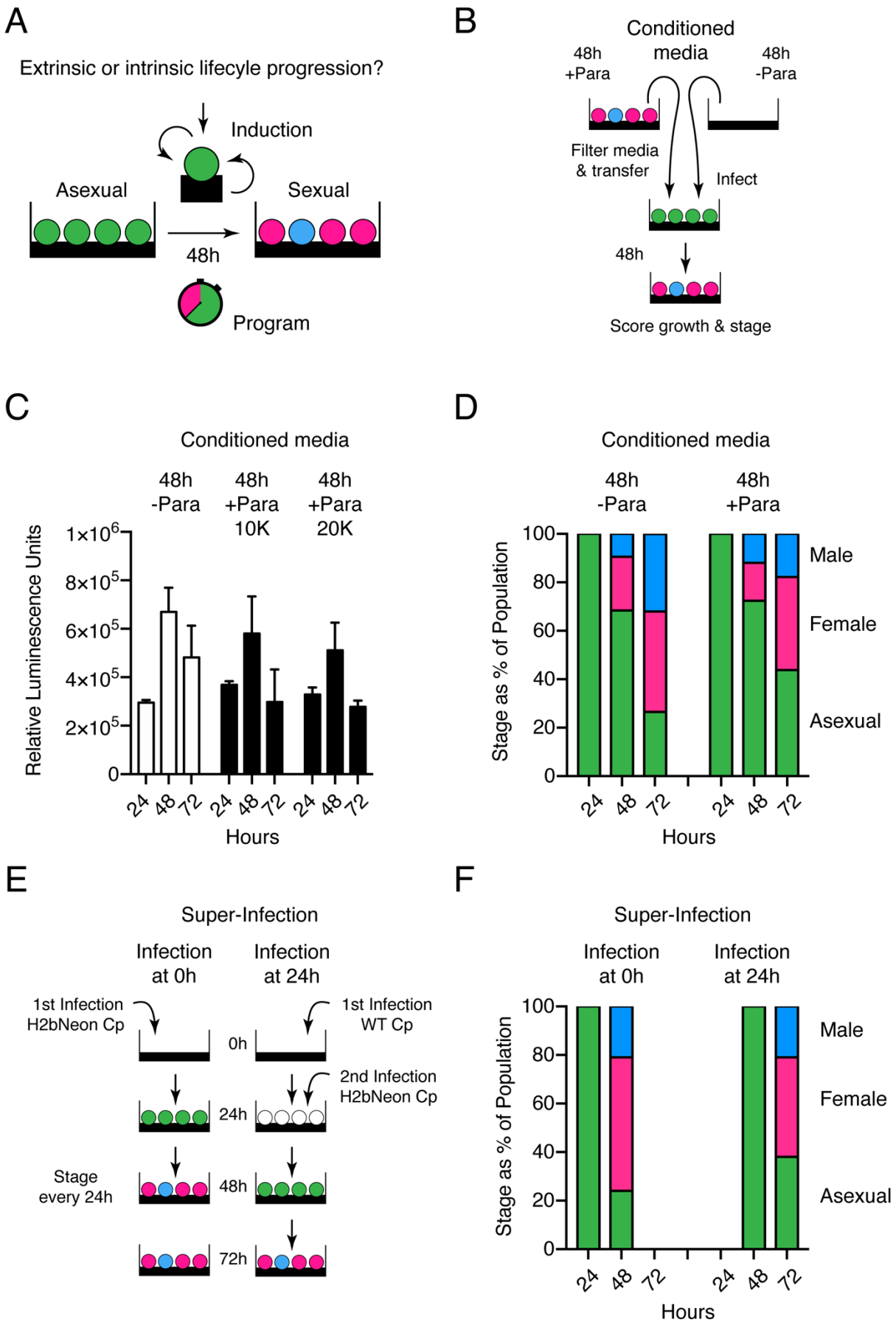

758 **Fig 1. Sexual differentiation of *C. parvum* is not dependent upon a secreted factor. (A)**
759 Schematic representation of both the induction and program hypotheses of *C. parvum* sexual
760 differentiation. **(B)** Schematic representation of the conditioned media experiment. Briefly, media
761 was conditioned for 48 hours in the presence of HCT-8 host cells with or without *C. parvum*
762 infection. Conditioned media was passed through a 0.45 μm filter and then used for new infections
763 that were scored for growth (C) and sexual differentiation (D). **(C)** Growth assay by luminescence
764 for *C. parvum* growth in conditioned media. **(D)** Stage scoring of *C. parvum* at 24, 48 and 72 hours
765 post infection when grown in conditioned media. **(E)** Schematic representation of super-infection
766 experiment. Briefly, HCT-8 cells were infected with H2BmNeon parasites that were previously
767 infected for 24 hours with wildtype parasites, or not previously infected. Both the primary infection
768 (WT) and super infection (H2BmNeon) were scored for parasite life stage at indicated time points
769 post infection. **(F)** Stage scoring and life cycle progression of *C. parvum* super-infection
770 experiment.
771

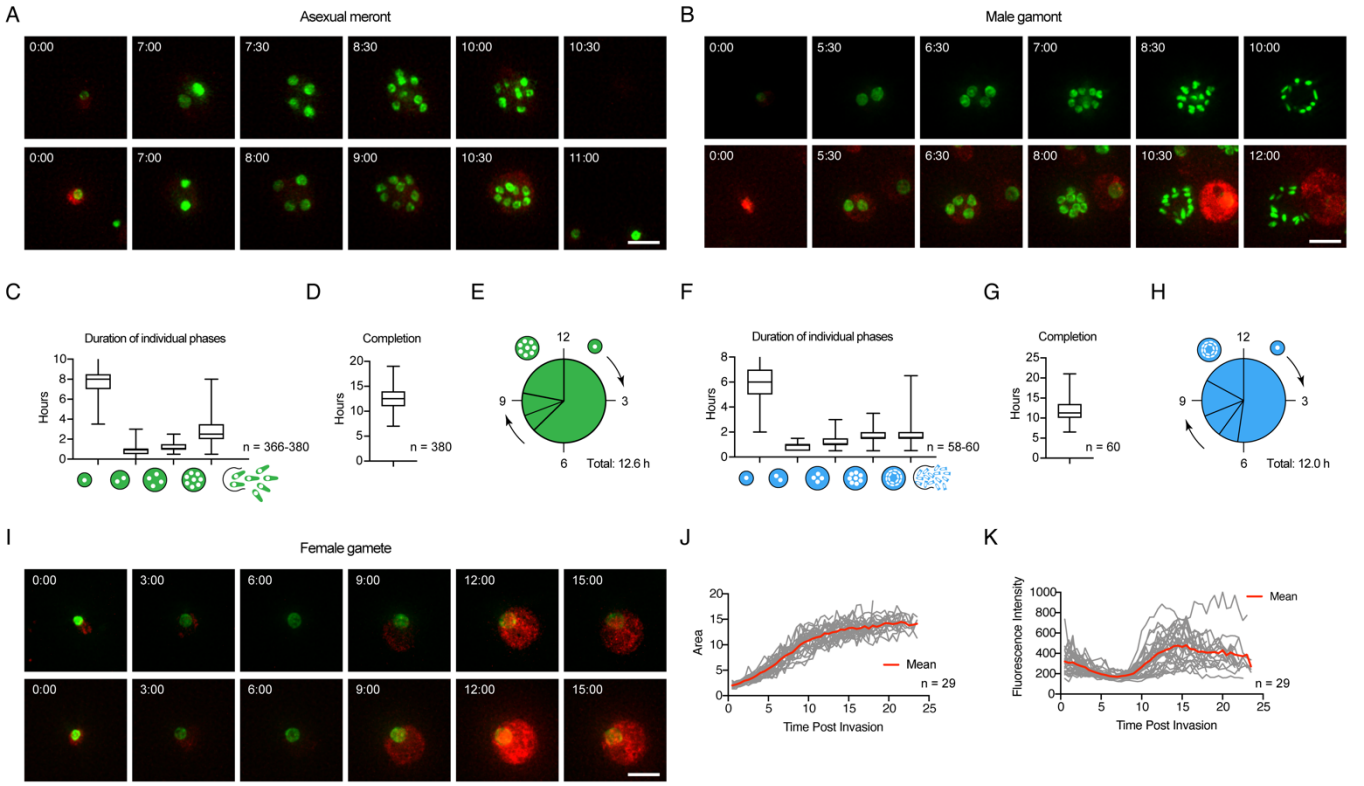

Fig 2. The intracellular development of all stages can be observed in real time in living cells. **(A)** Images taken from time lapse microscopy depicting asexual growth and nuclear division, two representative meronts. Scale bar 5 μm. **(B)** Images taken from time lapse microscopy depicting male parasite growth and nuclear division, two representative gamonts. Scale bar 5 μm. **(C)** Duration of phases of asexual growth. Parasites remain as a single nucleus for an average of 7.92 hours, followed by 0.83 hours as 2 nuclei, 1.11 hours as 4 nuclei, and 2.77 hours as 8 nuclei prior to egress (n= 366-380). **(D)** Asexual parasites remain intracellular (invasion to egress) for an average of 12.57 hours (n=380). **(E)** Graphical representation of the timing of nuclear divisions during asexual development. **(F)** Duration of phases of male growth. Parasites remain as a single nucleus for an average of 6.28 hours, followed by 0.92 hours as 2 nuclei, 1.07 hours as 4 nuclei, and 1.69 hours as 8 nuclei, and 2.05 hours as 16 nuclei prior to egress (n= 58-60). **(G)** Male parasites remain intracellular (invasion to egress) for an average of 12.08 hours (n=60). **(H)** Graphical representation of the timing of nuclear divisions during male development.

786 **(I)** Images taken from time lapse microscopy depicting female growth, two representative
787 gametes. Scale bar 5 μm. **(J)** Total area of female parasites over time. Grey lines represent
788 individual female parasites, red line indicates the average area of female parasites over time
789 (n=29). **(K)** Total fluorescent intensity of cytoplasmic mScarlet for the entire area of female
790 parasites over time. Grey lines represent individual female parasites, red line indicates the
791 average of female parasite over time (n=29).
792

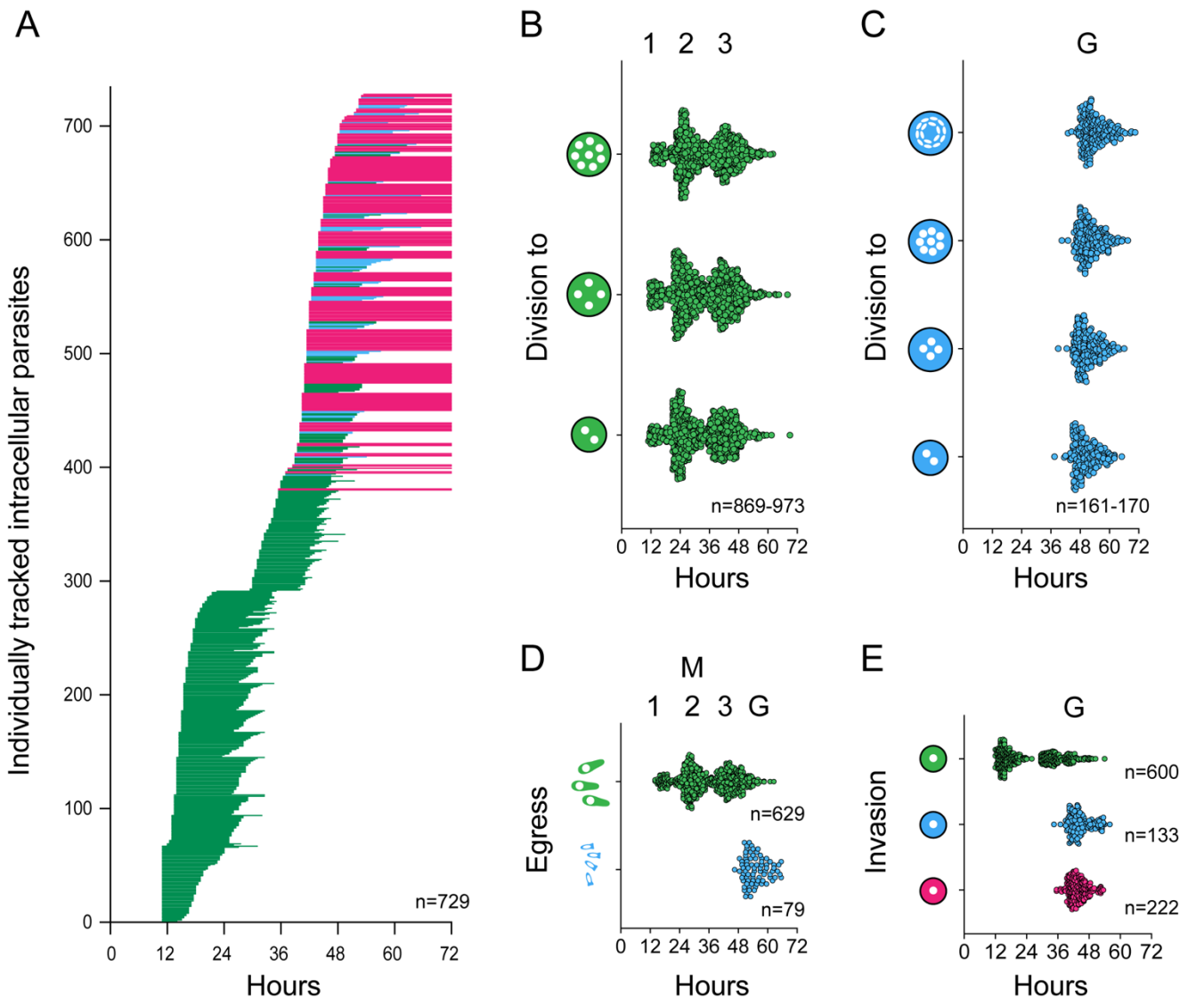

Fig 3. Extended time-lapse imaging reveals three cycles of asexual schizogony followed by differentiation into gametes. (A) Individually tracked parasites over time. Each horizontal line represents an individual parasite from invasion to egress (green= asexual, blue= male, pink= female). Lines for females cut off at 72 hours, as we do not observe egress of these parasites. Parasites with observed egress, but which invaded prior to the start of the experiment are included with lines beginning at 11 hours (n=729). **(B)** Individually plotted nuclear division events for asexual parasites over time. The time point at which we observe 2, 4, or 8 nuclei for the first time for parasites designated as asexual are plotted as individual points over time (n=869-973). **(C)**

802 Individually plotted nuclear division events for male parasites over time. The time point at which
803 we observe 2, 4, 8, or 16 nuclei for the first time for parasites designated as male are plotted as
804 individual points over time (n=161-179). **(D)** Individually plotted egress events for both asexual
805 (green) and male (blue) parasites over time. The time at which we no longer observe a parasite
806 is designated the time of egress. Each point represents a single asexual meront or male gamont.
807 There are 3 distinct clusters of asexual egress events, and a single cluster of male egress events
808 (asexual n=629, male n=79). **(E)** Individually plotted invasion events for asexual (green), male
809 (blue), and female (pink) parasites over time. The time at which a parasite is first observed is
810 considered the time of invasion. There are two observed clusters of invasion events leading to
811 asexual parasites, and only one cluster leading to male or female cells, respectively (asexual
812 n=600, male n=133, female n=222).
813

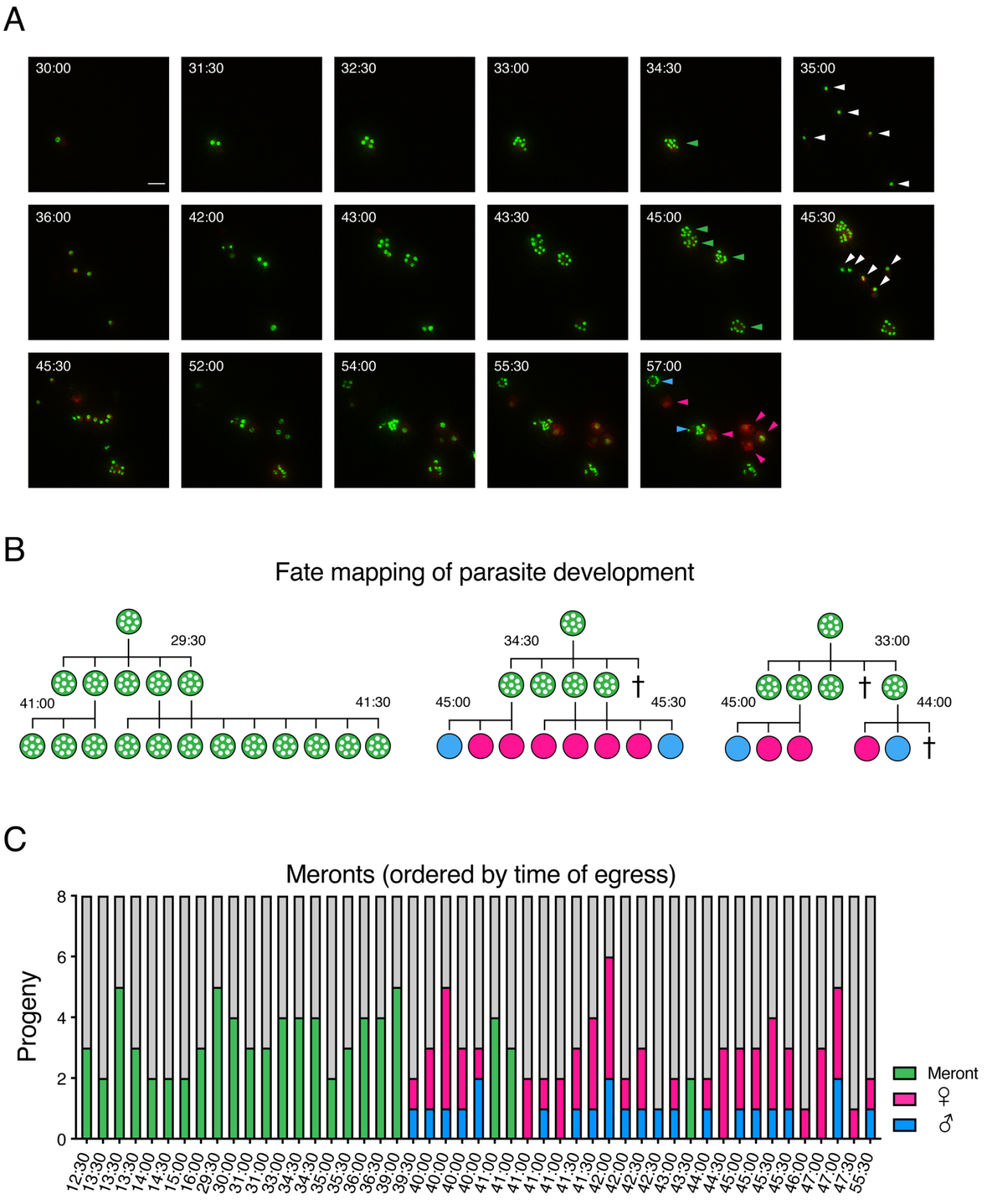

Fig 4. Meronts commit their merozoites to either asexual or sexual fate, but when committed to sex give rise to both males and females. (A) Images taken from time lapse

817 microscopy depicting multiple generations of parasite replication, including both asexual and
818 sexual stage growth and development. Stills take from video (see S4 Movie) over 27 hours of
819 observation. Green arrows indicate final fate of asexual meronts, white arrows indicate newly
820 invaded parasites immediately following an egress event. Blue arrows indicate parasites
821 designated with a male fate, pink arrows indicate parasites designated with a female fate. Scale
822 bar 5 μm. **(B)** Representative trees depicting the mapped fate of parasites for which the fate of
823 progeny of a single parental meront could be tracked. The tree in the center represents the images
824 seen in (A). **(C)** Fate of progeny of single meronts, ordered by time of egress. For each parental
825 meront, the fate of all observable progeny was tracked and is indicated (asexual=green,
826 male=blue, female=pink). Individual parental meronts are ordered by the time at which the
827 parental meront was last observed.
828

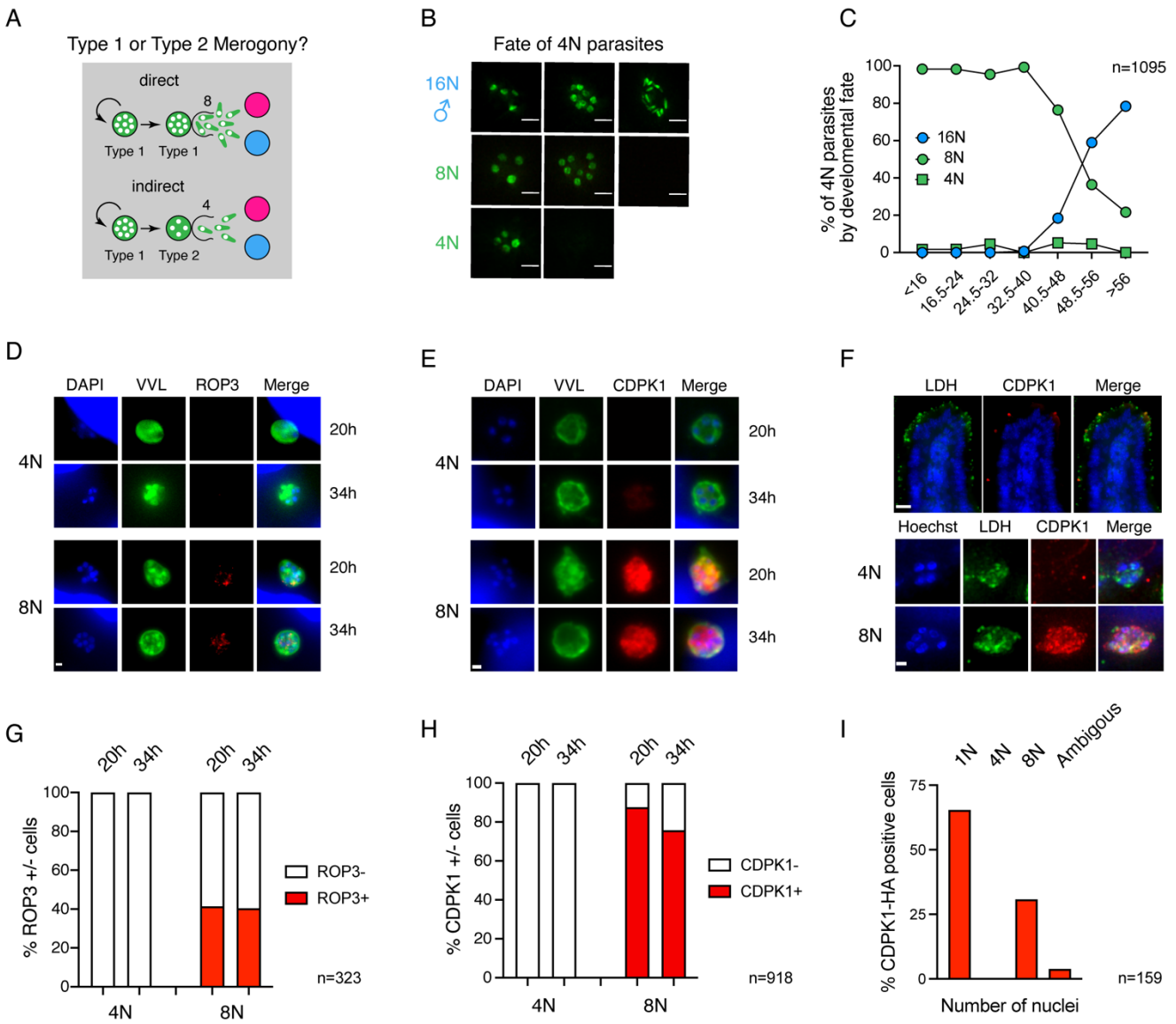

Fig 5. Development to gametes occurs directly from type one meronts and there is no evidence to support a 4N type two meront as the committed stage. (A) Schematic depicting hypotheses of life cycle progression. Parasites might undergo direct development in which Type I meronts producing 8 progeny develop into sexual stages or indirect development in which an intermediary Type II meront producing only 4 progeny gives rise to sexual stages. **(B)** Images depicting the possible fates of parasites that progress through a stage with 4 nuclei. Parasites were assigned 3 fates: 1) Those that progress from 4, to 8, and eventually 16 nuclei are male 2) Those that progress from 4 to 8 nuclei are asexual Type I meronts, and 3) Those that appear to

egress as 4 nuclei are asexual Type II meronts. Parasites which remained as 4 nuclei until the end of the experiment were excluded from this analysis. **(C)** Graph of the fate of 4N parasites over time. Prior to 16 hours of infection nearly 100% of the parasites that pass through a 4N stage become 8N prior to egress. This decrease after 40.5 hours of infection, and this decrease is proportional to the increase in parasites that become 16N (male) at these time points (n=1095). **(D** and **E)** Immunofluorescence of HCT-8 cells infected with transgenic *C. parvum* expressing ROP3-HA or CDPK1-HA, respectively. Representative images of 4N or 8N meronts at 20 and 34 hours post infection are shown. Only parasites with 8 nuclei express ROP3 (D) or CDPK1 (E) at either time point. Scale bar 1 μm. **(F)** Ifn$\gamma^{-/-}$ mice were infected with CDPK1-HA parasites and immunofluorescence staining was conducted on frozen sections of the small intestine. Top, low magnification micrograph of a highly infected segment of the intestinal tissue. Scale bar 15 μm. All parasite stages are labelled with an antibody to LDH (green) and mature meronts ready to egress are labeled with CDPK1 (red). Bottom, higher magnification images of 4N or 8N parasite. Parasites with 8 nuclei but not 4 nuclei express CDPK1 *in vivo*. Scale bar 1 μm. **(G)** Quantification of the ROP3 positive meronts for the entire 4N or 8N population at 20 and 34 hours post infection. **(H)** Quantification of the CDPK1 positive meronts at 20 and 34 hours post infection. (**I**) Quantification of the number of nuclei of a total of 159 CDPK1 positive parasites observed in 26 independent fields of view of intestinal sections. Only young 1N trophozoite and meronts 8 nuclei were positive for CDPK1 and matching our studies in culture we did not observe a single positive tetraploid parasite.

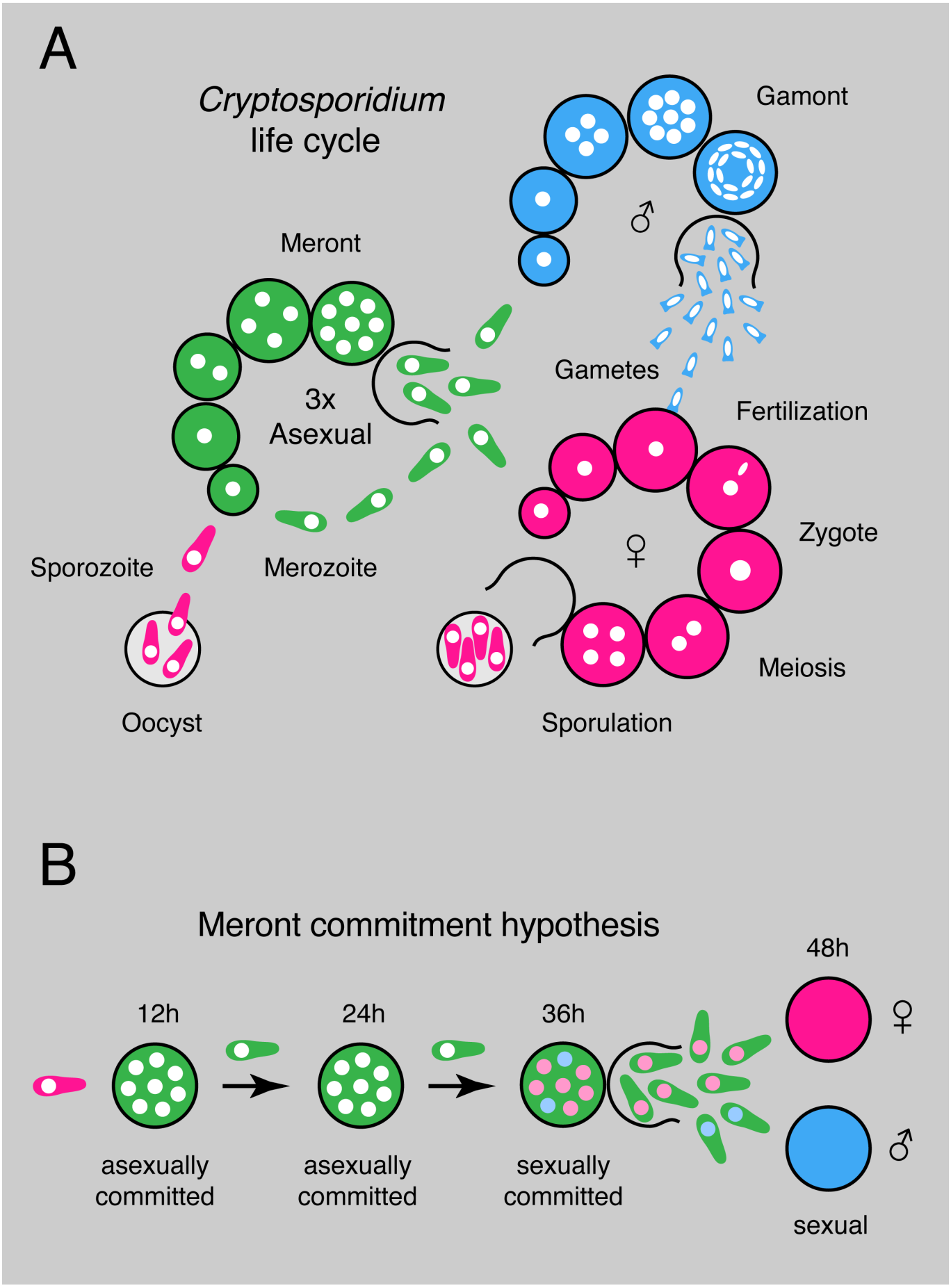

Fig 6. Model of *Cryptosporidium* life cycle and sexual commitment. (A) Schematic representation of the life cycle for *Cryptosporidium* summarizing the findings of this study. Infection begins with the oocyst which releases four sporozoites that invade intestinal epithelial cells. The parasites replicate asexually (green) by synchronous schizogony for three cycles and invariantly produce eight merozoites. Merozoites emerging from the third round upon reinvasion give rise to sexual stages, both males (blue) and female (pink). The male gamont undergoes four rounds of synchronous nuclear division producing 16 gametes, while the female gamete is cell cycle arrested and remains haploid while expanding in size and stockpiling proteins, lipids, and carbohydrates for the future oocyst. Male gametes egress and fertilize intracellular female gametes. Following fertilization, meiosis, and sporulation oocyst are released from the host cell that are immediately infectious. Oocyst can be shed with the feces resulting in transmission or excyst and reinfect the same host. (**B**) We propose a developmental commitment model of lifecycle progression for *Cryptosporidium*. Merozoites emerging a merogony cycle are collectively committed to an asexual or sexual fate, and when sexually committed give rise to both male and females (commitment is represented symbolically here by coloring the nuclei forestalling future fate, however, we note that the mechanism is unknown and may be independent of the nucleus).

878 **Supporting information**

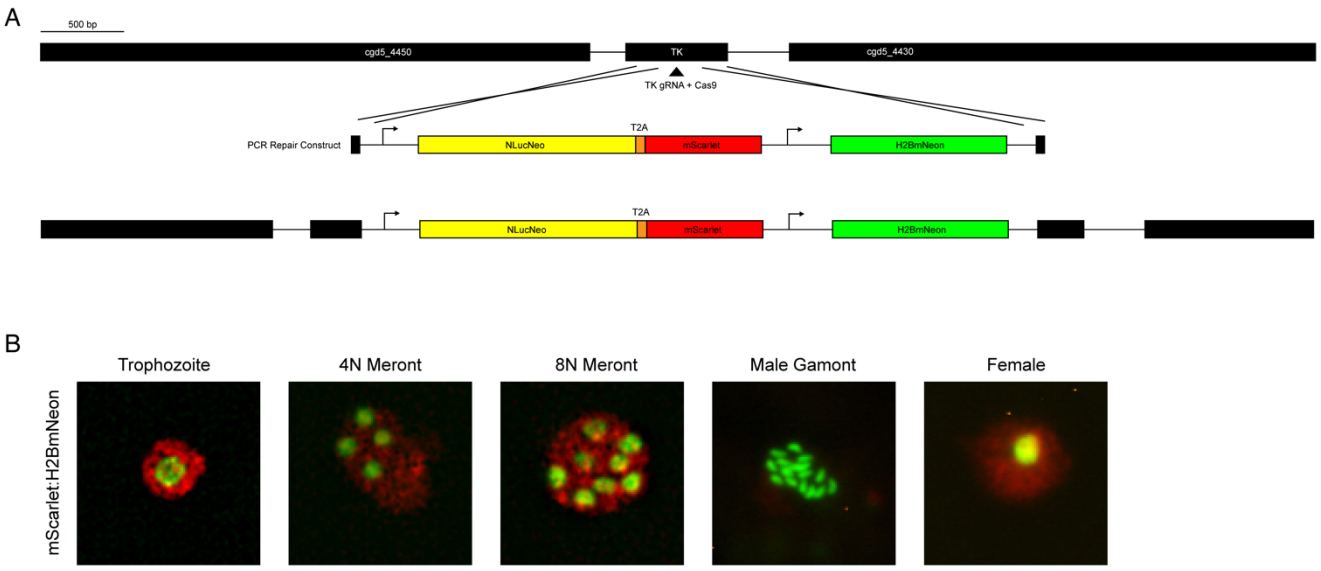

879

880 **S1 Fig. Generation of mScarlet-H2BmNeon parasites. (A)** Schematic overview of the guide
881 and repair constructs used to generate the transgenic parasite line with a cytosolic mScarlet and
882 a nuclear mNeon inserted into the TK locus. **(B)** Visualization of the fluorescent protein localization
883 in multiple life stages for the mScarlet-H2BmNeon transgenic parasites.

884

885

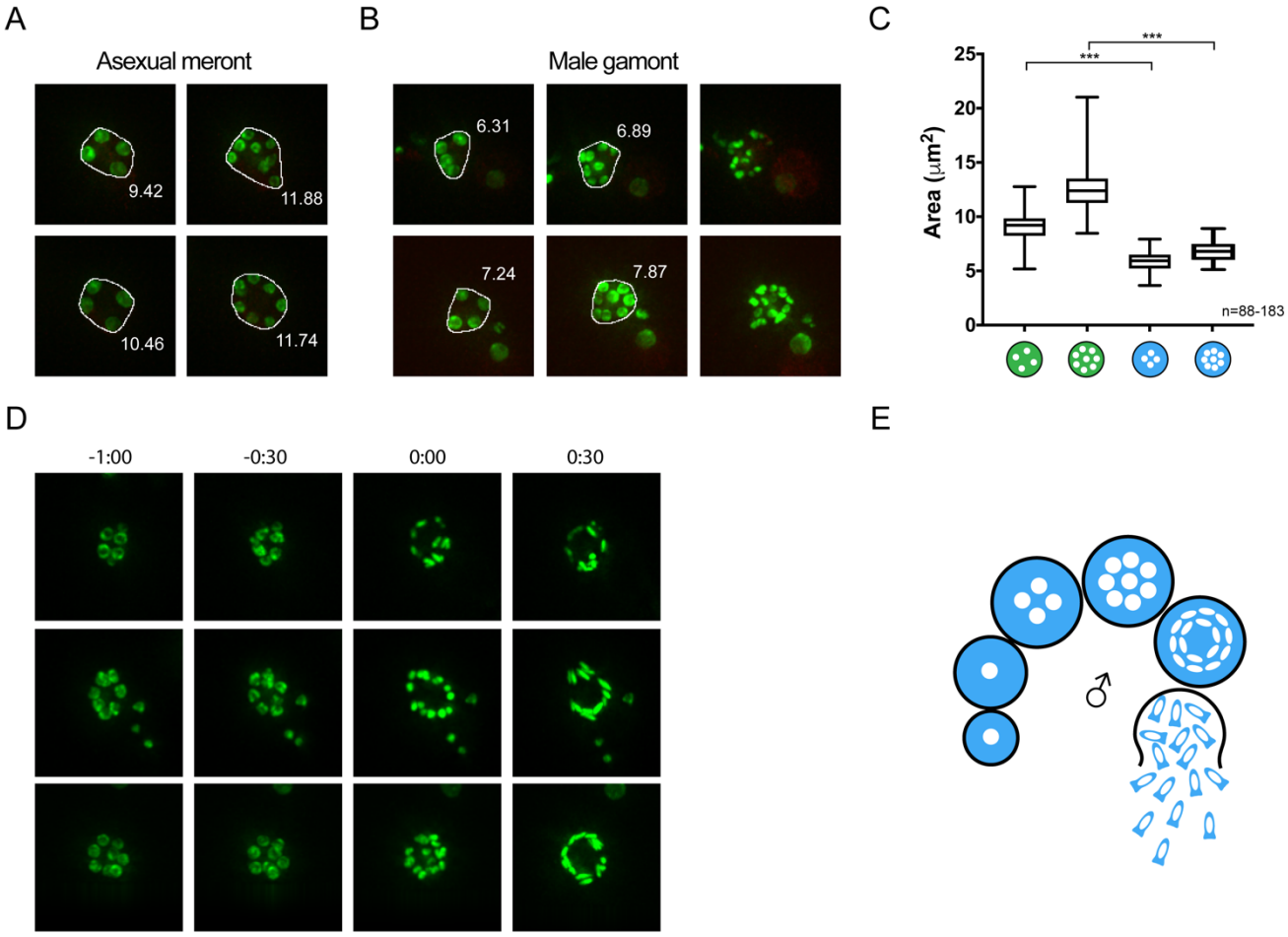

886

887 **S2 Fig. The nuclei of dividing male parasites cluster closer together than those of dividing**
888 **asexual parasites. (A)** Two representative images depicting asexual parasites at 4 and 8 nuclei,
889 including the boundary drawn around all nuclei to measure nuclear spread. The area for each
890 meront is included. **(B)** Representative images depicting male parasites at 4, 8 and then 16 nuclei,
891 including the boundary drawn around all nuclei at 4 and 8 nuclei stages to measure nuclear
892 spread. The area for each gamont is included. **(C)** Comparison of the area of nuclear spread for
893 asexual and male parasites with 4 or 8 nuclei. The area taken up by male nuclei is significantly
894 smaller than the area taken up by asexual nuclei at both the 4 and 8 nuclei stages (Welch's T-
895 test, *** $p < 0.0001$). **(D)** Three representative image series of male nuclear development. Nuclei

remain round when 8 nuclei are present and adopt distinct bullet-like male shape only after dividing to 16 nuclei.

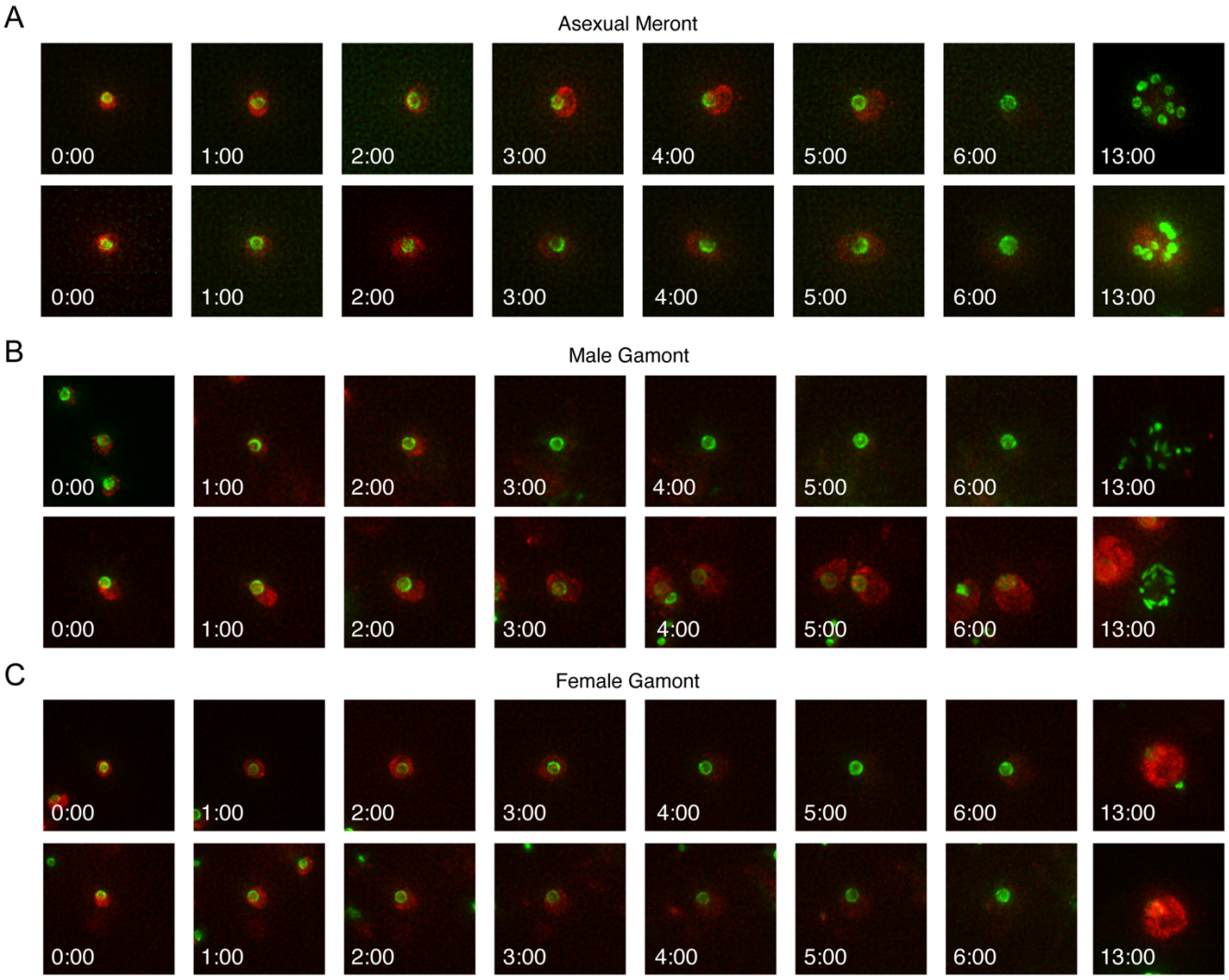

S3 Fig. The establishment phase of asexual, male, and female parasites is visually indistinguishable for the first 6 hours of infection. (A) Images from two representative asexual meronts shown every hour for the first six hours, followed by a 13 hours time point to confirm stage. **(B)** Images from two representative male gamonts shown every hour for the first six hours, followed by a 13 hours time point to confirm stage. **(C)** Images from two representative female gamonts shown every hour for the first six hours, followed by a 13 hours time point to confirm stage.

S1 Movie. Growth and division of asexual *C. parvum*. Five representative videos of individual asexual meronts from first appearance to apparent egress.

S2 Movie. Growth and division of male *C. parvum*. Five representative videos of individual male gamonts from first appearance to apparent egress.

S3 Movie. Growth and development of female *C. parvum*. Five representative videos of individual female gamonts from first appearance until maximum fluorescence intensity has passed.

S4 Movie. Multiple generations of asexual growth and sexual development of *C. parvum*. A representative image of two generations of asexual growth, followed by the development of male and female gamonts.